Received October 29, 2015, accepted November 18, 2015. Date of publication xxxx 00, 0000, date of current version xxxx 00, 0000.

Digital Object Identifier 10.1109/ACCESS.2015.2503267

Fifteen Years of Quantum LDPC Coding and Improved Decoding Strategies

ZUNAIRA BABAR, PANAGIOTIS BOTSINIS, (Student Member, IEEE), DIMITRIOS ALANIS, (Student Member, IEEE), SOON XIN NG, (Senior Member, IEEE), AND LAJOS HANZO, (Fellow, IEEE)

School of Electronics and Computer Science, University of Southampton, Southampton SO17 1BJ, U.K.

Corresponding author: L. Hanzo (lh@ecs.soton.ac.uk)

AQ:1 This work was supported by the European Research Council Advanced Fellow Grant through the Engineering and Physical Sciences Research Council U.K. under Grant EP/L018659/1.

ABSTRACT The near-capacity performance of classical low-density parity check (LDPC) codes and their efficient iterative decoding makes quantum LDPC (QLPDC) codes a promising candidate for quantum error correction. In this paper, we present a comprehensive survey of QLDPC codes from the perspective of code design as well as in terms of their decoding algorithms. We also conceive a modified non-binary decoding algorithm for homogeneous Calderbank–Shor–Steane-type QLDPC codes, which is capable of alleviating the problems imposed by the unavoidable length-four cycles. Our modified decoder outperforms the state-of-the-art decoders in terms of their word error rate performance, despite imposing a reduced decoding complexity. Finally, we intricately amalgamate our modified decoder with the classic uniformly reweighted belief propagation for the sake of achieving an improved performance.

INDEX TERMS Quantum error correction, low density parity check codes, quantum low density parity check codes, iterative decoding.

NOMENCLATURE

AWGN	Additive White Gaussian Noise
BER	Bit Error rate
BIBD	Balanced Incomplete Block Design
BSC	Binary Symmetric Channel
BP	Belief Propagation
CSS	Calderbank-Shor-Steane
EA	Entanglement-Assisted
EAP	Edge Appearance Probability
EG	Euclidean Geometry
FAP	Factor Appearance Probability
FFT	Fast Fourier Transform
LDGM	Low Density Generator Matrix
LDPC	Low Density Parity Check
PCM	Parity Check Matrix
PDF	Probability Density Function
QBER	Qubit Error rate
QC	Quasi-Cyclic
QECC	Quantum Error Correction Code
QLDPC	Quantum Low Density Parity Check
QSC	Quantum Stabilizer Code
QTC	Quantum Turbo Code
RX	Receiver
SC	Spatially-Coupled
SPA	Sum-Product Algorithm
TRW-BP	Tree-Reweighted Belief Propagation
TX	Transmitter
URW-BP	Uniformly-Reweighted Belief Propagation
WER	Word Error Rate

I. INTRODUCTION

Operating close to Shannon's channel capacity limit is only feasible under the idealized conditions of perfect synchronization, perfect channel estimation and in case of potentially infinite delay/complexity channel codes. It was demonstrated in [1] that only a fraction of the theoretical limit is achievable in realistic scenarios. The logarithmic increase in the idealized Shannonian capacity with the transmit power imposes another limitation. Nevertheless, provided that we can create a sufficiently high number of parallel streams and that we have a low-complexity full-search based multi-stream detector, the throughput of the wireless system may be increased linearly with the transmit power. Unfortunately, the associated optimal full-search-based multi-stream detectors have an excessive complexity, which increases exponentially both with the number of users as well as with that of the antennas. Since quantum-based parallel computation is capable of solving certain complex problems at a substantially lower complexity than its classical counterpart, quantum parallel processing techniques may be invoked [2]–[6]. The peculiar laws of quantum mechanics have also spurred interest in quantum-based communication systems, which have given rise to a new range of security paradigms in the context of quantum key distribution techniques [7], [8], quantum secure direct communication [9], [10] and unconditional quantum location verification [11].

Unfortunately, quantum noise, conventionally termed as 'decoherence', imposes a hitherto insurmountable impairment on the practical implementation of quantum computation as well as on quantum communication systems. More precisely, decoherence is the undesirable interaction of the constituent qubits[1] with the environment, which perturbs the superposition of states [13], [14]. For the sake of having a reliable quantum computation or communication system, it is desired to counteract the above-mentioned decoherence so that the qubits retain their coherent quantum states for practical durations. Since decoherence may be characterized either by bit-flips or phase-flips or in fact possibly by both, Quantum Error Correction Codes (QECCs), designed for correcting both bit-flips as well as phase-flips, may be invoked for correcting the errors inflicted on the qubits [13].

The inception of QECCs dates back to 1995 when Shor [13] conceived the first quantum code, which was however only capable of correcting a single error. Since then the quest for approaching the quantum capacity bounds at an affordable encoding and decoding complexity has continued. In this context, the astounding performance of the classical Low Density Parity Check (LDPC) codes [15]–[19], which exhibit a near-capacity performance at an affordable decoding complexity, has inspired the community to design Quantum Low Density Parity Check (QLDPC) codes. The sparseness of the QLDPC matrix is of particular interest in the quantum domain, because it requires only a small number of interactions per qubit during the error correction procedure, thus facilitating fault-tolerant decoding.

QLDPC codes belong to the family of Quantum Stabilizer Codes (QSCs) [20], [21], which is a generalized formalism for designing quantum codes from any arbitrary classical binary and quaternary codes.[2] However, this transfiguration from the classical to the quantum domain imposes a stringent symplectic criterion on the parent classical codes, which brings with it various design challenges. Against this backdrop, in this paper we survey the evolution of QLDPC code designs, focusing on the various code constructions to conceive powerful QLDPC codes from the known families of classical LDPC codes. We also review the syndrome-based iterative decoding algorithms invoked for QLDPC codes. Finally, we conceive a modified non-binary decoding algorithm for homogeneous Calderbank-Shor-Steane (CSS)-type QLDPC codes, which is capable of mitigating the impact of the unavoidable length-4 cycles. Our modified decoder exhibits a superior Word Error Rate (WER) performance, despite its reduced decoding complexity, when compared to the state-of-the-art decoding techniques. We demonstrate furthermore that the Uniformly-Reweighted Belief Propagation (URW-BP) technique of [23] and [24] may also be invoked for further improving the attainable performance.

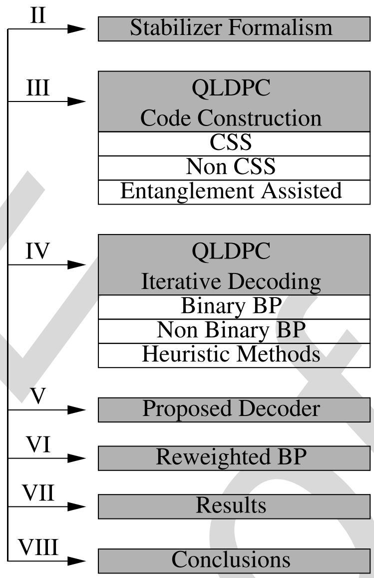

FIGURE 1. **Paper structure.**

This paper is organized as depicted in Fig. 1. We commence with a summary of the stabilizer code design formalism in Section II. We then proceed with a review of QLDPC code designs in Section III, while a range of powerful decoding techniques are discussed in Section IV. Finally, we present our proposed decoding algorithm in Section V, while in Section VI we detail the reweighted belief propagation philosophy. Our simulation results are presented in Section VII, while Section VIII concludes our discourse.

II. STABILIZER FORMALISM

Let us first state the important definitions used for describing the stabilizer code formalism [25].

A. PAULI OPERATORS

The **I**, **X**, **Y** and **Z** Pauli operators are defined by the following matrices:

$$\mathbf{I} = \begin{pmatrix} 1 & 0 \\ 0 & 1 \end{pmatrix}, \quad \mathbf{X} = \begin{pmatrix} 0 & 1 \\ 1 & 0 \end{pmatrix},$$

$$\mathbf{Y} = \begin{pmatrix} 0 & -i \\ i & 0 \end{pmatrix}, \quad \mathbf{Z} = \begin{pmatrix} 1 & 0 \\ 0 & -1 \end{pmatrix}, \tag{1}$$

[1]In contrast to a classical bit, which can either assume a value of 0 or 1, a qubit can exist in a superposition of the two states represented as $|\psi\rangle = \alpha|0\rangle + \beta|1\rangle$. Here, $|\ \rangle$ is called Dirac notation or Ket [12], while α and β are complex numbers with $|\alpha|^2 + |\beta|^2 = 1$. More specifically, a qubit exists in a continuum of states between $|0\rangle$ and $|1\rangle$ until it is 'measured' or 'observed'. Upon 'measurement' it collapses to the state $|0\rangle$ with a probability of $|\alpha|^2$ and $|1\rangle$ with a probability of $|\beta|^2$.

[2]For a detailed description of the transition from the classical codes to the quantum codes, readers are referred to [22].

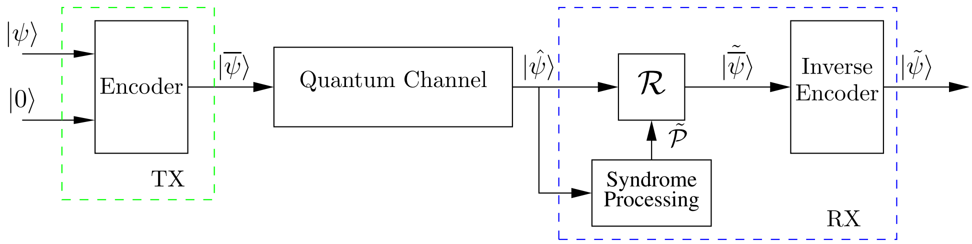

FIGURE 2. **General schematic of a quantum communication system.**

where the **X**, **Y** and **Z** operators anti-commute with each other.

B. PAULI GROUP

A single qubit Pauli group $\mathcal{G}_1$ is a group formed by the Pauli matrices **I**, **X**, **Y** and **Z**, which is closed under multiplication. Therefore, it consists of all the Pauli matrices together with the multiplicative factors ± 1 and $\pm i$, i.e. we have:

$$\mathcal{G}_1 \equiv \{\pm\mathbf{I}, \pm i\mathbf{I}, \pm\mathbf{X}, \pm i\mathbf{X}, \pm\mathbf{Y}, \pm i\mathbf{Y}, \pm\mathbf{Z}, \pm i\mathbf{Z}\}. \tag{2}$$

The general Pauli group $\mathcal{G}_n$ is an n-fold tensor product of $\mathcal{G}_1$.

C. DEPOLARIZING CHANNEL

A depolarizing channel, which is characterized by the probability p, inflicts an error $\mathcal{P} \in \mathcal{G}_n$ on n qubits, where each qubit may independently experience either a bit-flip (**X**), a phase-flip (**Z**) or both (**Y**) with a probability of $p/3$ each, when considering the default symmetric depolarizing channel.

Fig. 2 shows the general schematic of a quantum communication system. At the transmitter TX, an $[n, k]$ QSC, constructed over a code space $\mathcal{C}$, maps the information word (logical qubits) $|\psi\rangle \in \mathbb{C}^{2^k}$ onto the codeword (physical qubits) $|\overline{\psi}\rangle \in \mathbb{C}^{2^n}$ with the aid of $(n-k)$ auxiliary (also called ancilla) qubits initialized to the state $|0\rangle$. Here $\mathbb{C}^d$ denotes the d-dimensional Hilbert space. Furthermore, let $\mathcal{P} \in \mathcal{G}_n$ be the channel error inflicted on the transmitted codewords. Consequently, $|\hat{\psi}\rangle = \mathcal{P}|\overline{\psi}\rangle$ is the noisy codeword received at the receiver RX, which invokes a 3-step decoding procedure for recovering the intended transmitted information $|\psi\rangle$.

Unlike a classical decoder, which measures the received bit values, a quantum decoder cannot measure the received qubits without perturbing their superimposed quantum states. More specifically, qubits collapse to classical bits upon their measurement/observation. Therefore, inspired by the Parity Check Matrix (PCM)-based syndrome decoding of classical codes [26], a quantum decoder circumvents the associated measurement operation by observing the error syndromes without reading the actual quantum information. In the context of an $[n, k]$ QSC, this is achieved by a set of $(n-k)$ independent commuting Pauli generators $g_i \in \mathcal{G}_n$, for $1 \leq i \leq (n-k)$. The corresponding stabilizer group $\mathcal{H}$ contains both g_i and all the products of g_i for $1 \leq i \leq (n-k)$ and forms an Abelian subgroup of $\mathcal{G}_n$. A unique feature of these generators is that they do not change the state of valid codewords, while yielding an eigenvalue of -1 for the corrupted states.[3] Consequently, the eigenvalue is -1 if $\mathcal{P}$ anti-commutes with the stabilizer g_i and it is $+1$ if $\mathcal{P}$ commutes with g_i, which can be formulated as:

$$g_i|\hat{\psi}\rangle = \begin{cases} |\overline{\psi}\rangle, & g_i\mathcal{P} = \mathcal{P}g_i \\ -|\overline{\psi}\rangle, & g_i\mathcal{P} = -\mathcal{P}g_i. \end{cases} \tag{3}$$

The resultant ± 1 eigenvalue gives the corresponding error syndrome, which is 0 for an eigenvalue of $+1$ and 1 for an eigenvalue of -1. Hence, within the 'syndrome processing' block of Fig. 2, the receiver RX computes the syndrome of the received sequence $|\hat{\psi}\rangle$ and uses it to estimate the channel-induced error pattern $\tilde{\mathcal{P}}$. The recovery operator $\mathcal{R}$ then uses the estimated error pattern $\tilde{\mathcal{P}}$ to restore the potentially error-free transmitted coded stream. It must be mentioned here that those channel errors, which differ only by the stabilizer group, have the same impact on all the codewords and therefore can be corrected by the same recovery operation. This equips quantum codes with the intrinsic property of degeneracy [27]. More explicitly, the error patterns $\mathcal{P}$ and $\mathcal{P}' = g_i\mathcal{P}$ have the same impact on the transmitted codeword and therefore can be corrected by the same recovery operation.[4] Finally, the 'inverse encoder' shown in Fig. 2, processes the recovered coded sequence $|\tilde{\overline{\psi}}\rangle$, yielding the estimated transmitted information qubits $|\tilde{\psi}\rangle$.

QSCs may be characterized in terms of an equivalent binary parity check matrix notation satisfying the commutativity constraint of the stabilizer generators [28], [29]. This is achieved by mapping the **I**, **X**, **Y** and **Z** Pauli operators onto $(\mathbb{F}_2)^2$ as follows:

$$\mathbf{I} \rightarrow (0,0), \quad \mathbf{X} \rightarrow (0,1), \ \mathbf{Y} \rightarrow (1,1), \ \mathbf{Z} \rightarrow (1,0). \tag{4}$$

[3]For example, consider a 3-qubit bit-flip repetition code, which encodes $|\psi\rangle = \alpha|0\rangle + \beta|1\rangle$ into $|\overline{\psi}\rangle = \alpha|000\rangle + \beta|111\rangle$, and has the generators $g_1 = \mathbf{ZZI}$ and $g_2 = \mathbf{ZIZ}$. Both g_1 as well as g_2 do not affect a valid codeword, i.e. $g_1[|\overline{\psi}\rangle] = g_2[|\overline{\psi}\rangle] = |\overline{\psi}\rangle$. On the other hand, let the received codeword be $|\hat{\psi}\rangle = \alpha|010\rangle + \beta|101\rangle$, then we get $g_1[|\overline{\psi}\rangle] = -|\overline{\psi}\rangle$, while $g_2[|\overline{\psi}\rangle] = |\overline{\psi}\rangle$. Therefore, the resulting syndromes are 1 and 0, respectively.

[4]For the 3-qubit bit-flip repetition code, let $\mathcal{P} = \mathbf{IIX}$ and $\mathcal{P}' = g_1\mathcal{P} = \mathbf{ZZX}$ be the errors inflicted by the channel. Both $\mathcal{P}$ as well as $\mathcal{P}'$ corrupt the transmitted codeword $|\overline{\psi}\rangle = \alpha|000\rangle + \beta|111\rangle$ to $|\hat{\psi}\rangle = \alpha|001\rangle + \beta|110\rangle$. Consequently, the errors $\mathcal{P}$ and $\mathcal{P}'$ need not be differentiated and are therefore classified as degenerate errors.

Based on this Pauli-to-binary isomorphism, the $(n-k)$ stabilizers of an $[n, k]$ stabilizer code constitute the rows of the binary PCM H, which is a concatenation of a pair of $(n-k) \times n$ binary matrices H_z and H_x, as given below:

$$H = (H_z|H_x)\,. \tag{5}$$

Each row of H corresponds to a stabilizer of $\mathcal{H}$, so that the ith columns of H_z and H_x are used to compute the error imposed on the ith qubit. More specifically, a binary 1 in the ith column of H_z (or H_x) represents a $\mathbf{Z}$ (or $\mathbf{X}$) Pauli operator in the corresponding stabilizer. Furthermore, given the matrix notation of Eq. (5), the commutative property of stabilizer generators is transformed into the orthogonality of rows with respect to the symplectic product (also referred to as a twisted product). If row i is $H_i = (H_{z_i}, H_{x_i})$, where H_{z_i} and H_{x_i} are the binary strings for $\mathbf{Z}$ and $\mathbf{X}$ respectively, then the symplectic product of rows i and i' is given by,

$$H_i \star H_{i'} = (H_{z_i} \cdot H_{x_{i'}} + H_{z_{i'}} \cdot H_{x_i}) \bmod 2. \tag{6}$$

The symplectic product of Eq. (6) is zero, if there are an even number of places in the generators g_i and $g_{i'}$ with different non-Identity (i.e. $\mathbf{X}$, $\mathbf{Y}$, or $\mathbf{Z}$) operators; thus meeting the commutativity requirement.[5] We may further deduce from Eq. (6) that if H is expressed as $H = (H_z|H_x)$, then the symplectic product is satisfied for all the rows of H if and only if we have:

$$H_z H_x^T + H_x H_z^T = 0. \tag{7}$$

Consequently, any classical code satisfying Eq. (7) may be used for constructing QSCs.

A special class of stabilizer codes is constituted by the family of CSS codes, invented independently by Calderbank and Shor [30] as well as by Steane [31], [32], which facilitates the design of high-performance quantum codes from the known family of classical binary linear codes. More explicitly, a $[n, k_1 - k_2]$ CSS code, which is capable of correcting t bit-flips as well as phase-flips, can be constructed from the classical linear block codes $C_1(n, k_1)$ and $C_2(n, k_2)$, if we have $C_2 \subset C_1$, and both C_1 and the dual of C_2, i.e. $C_2^\perp$, can correct t errors. In CSS construction, the PCM H_z' of C_1 is used for correcting bit-flips, while the PCM H_x' of $C_2^\perp$ is used for phase-flip correction. Consequently, the PCM of the resultant CSS code assumes the following form:

$$H = \begin{pmatrix} H_z' & \mathbf{0} \\ \mathbf{0} & H_x' \end{pmatrix}, \tag{8}$$

where we have $H_z = \begin{pmatrix} H_z' \\ \mathbf{0} \end{pmatrix}$, $H_x = \begin{pmatrix} \mathbf{0} \\ H_x' \end{pmatrix}$ and both H_z' and H_x' are $(n-k_1) \times n$ and $k_2 \times n$ binary matrices, respectively. Furthermore, since we have $C_2 \subset C_1$, the symplectic condition of Eq. (7) is reduced to $H_z' H_x'^T = 0$. For the specific case where $H_z' = H_x'$, the resultant structure is termed as a dual-containing (or self-orthogonal) code because $H_z' H_z'^T = 0$, which is equivalent to $C_1^\perp \subset C_1$.

TABLE 1. GF(4) addition.

+	0	1	ω	$\overline{\omega}$
0	0	1	ω	$\overline{\omega}$
1	1	0	$\overline{\omega}$	ω
ω	ω	$\overline{\omega}$	0	1
$\overline{\omega}$	$\overline{\omega}$	ω	1	0

AQ:2

TABLE 2. GF(4) multiplication.

$\times$	0	1	ω	$\overline{\omega}$
0	0	0	0	0
1	0	1	ω	$\overline{\omega}$
ω	0	ω	$\overline{\omega}$	1
$\overline{\omega}$	0	$\overline{\omega}$	1	ω

Since the $\mathbf{I}$, $\mathbf{X}$, $\mathbf{Y}$ and $\mathbf{Z}$ Pauli operators have the equivalent 2-bit representation of Eq. (4), they may also be expressed in the Galois Field GF(4) by the equivalent 4-ary symbols. More specifically, the Pauli-to-GF(4) isomorphism may be encapsulated as:

$$\mathbf{I} \to 0, \quad \mathbf{X} \to 1, \ \mathbf{Y} \to \overline{\omega}, \ \mathbf{Z} \to \omega, \tag{9}$$

where $0, 1, \omega$ and $\overline{\omega}$ are the elements of GF(4), which conform to the additive and multiplicative rules of Table 1 and Table 2, respectively. According to the Pauli-to-GF(4) isomorphism, the multiplication of Pauli operators is transformed into the addition of the corresponding elements in GF(4), while the commutativity (symplectic product) criterion is mapped onto the trace[6] inner product [21]. For example, multiplying the set of Pauli operators $\{\mathbf{I}, \mathbf{X}, \mathbf{Z}, \mathbf{Y}\}$ with Pauli-$\mathbf{X}$ is equivalent to the second column of Table 1. Furthermore, the commutative relationship between $\hat{A}$ and $\hat{B}$ in GF(4) is computed using the trace inner product as follows[7]:

$$\mathrm{Tr}\langle \hat{A}, \hat{B} \rangle = \mathrm{Tr}(\hat{A} \times \overline{\hat{B}}) = 0, \tag{10}$$

where $\langle , \rangle$ represents the Hermitian inner product and $\overline{\hat{B}}$ denotes the conjugate[8] of $\hat{B}$. Furthermore, $\mathrm{Tr}(0) = \mathrm{Tr}(1) = 0$, while $\mathrm{Tr}(\omega) = \mathrm{Tr}(\overline{\omega}) = 1$. Consequently, based on Eq. (10), the symplectic product of Eq. (6) is transformed into the trace inner product in GF(4). For example, the symplectic product of the ith and i'th row of $\hat{H}$, which is defined in GF(4), is formulated as:

$$\hat{H}_i \star \hat{H}_{i'} = \mathrm{Tr}\left(\hat{H}_i \cdot \hat{H}_{i'}\right) = \mathrm{Tr}\left(\sum_{t=1}^{n} \hat{H}_{it} \times \overline{\hat{H}}_{i't}\right), \tag{11}$$

[5]For example, let $g_1 = \mathbf{XZI}$ and $g_2 = \mathbf{ZII}$, which have different non-Identity Pauli operators only at the first index. Then the generators g_1 and g_2 anti-commute. Alternatively, according to the binary mapping of Eq. (4), we have $g_1 \equiv (010|100)$, while $g_2 \equiv (100|000)$. Therefore, the symplectic product of Eq. (6) yields a value of 1. By contrast, if the generators are $g_1 = \mathbf{XZI}$ and $g_2 = \mathbf{ZXI}$, then they commute. Consequently, the symplectic product of Eq. (6) gives a value of zero.

[6]In GF(4), the trace operator maps x to $(x + \overline{x})$. where $\overline{x}$ is the conjugate of x [33].

[7]We denote GF(4) variables with a ˆ on top, e.g. $\hat{x}$.

[8]In GF(4), the conjugate operation swaps the elements ω and $\overline{\omega}$, while leaving 0 and 1 intact.

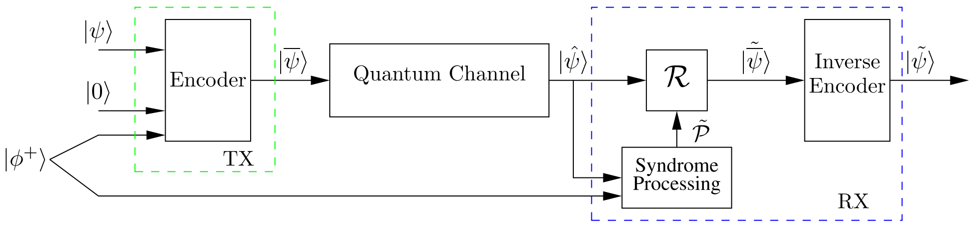

FIGURE 3. General schematic of an entanglement-assisted quantum communication system.

where $\hat{H}_{it}$ denotes the element in the ith row and tth column of $\hat{H}$.

TABLE 3. Quantum-to-classical isomorphism.

Pauli	$(\mathbb{F}_2)^2$	GF(4)
I	$(0, 0)$	0
X	$(0, 1)$	1
Y	$(1, 1)$	$\overline{\omega}$
Z	$(1, 0)$	ω
Multiplication	Bit-wise Addition	Addition
Commutativity	Symplectic Product	Trace Inner Product

Based on the above discussions, a Pauli operator may be expressed in terms of the equivalent binary or quaternary representation, which is summarized in Table 3. This in turn facilitates the design of quantum codes from the known classical codes. More explicitly, arbitrary classical binary and quaternary codes may only be used for constructing QSCs if they satisfy the commutativity criterion of Eq. (7). Consequently, some of the good classical codes cannot be exploited in the quantum domain. The entanglement-assisted stabilizer formalism of [34]–[37] overcomes this limitation by using pre-shared entanglement[9] between the transmitter and receiver to embed a set of non-commuting stabilizer generators into a larger set of commuting generators.

Fig. 3 shows the general schematic of a quantum communication system, which incorporates an Entanglement-Assisted Quantum Stabilizer Code (EA-QSC). An $[n, k, c]$ EA-QSC encodes the information qubits $|\psi\rangle$ into the coded sequence $|\overline{\psi}\rangle$ with the aid of $(n-k-c)$ auxiliary qubits, which are initialized to the state $|0\rangle$. Furthermore, the transmitter and receiver share c entangled qubits (ebits) before actual transmission takes place. This may be carried out outside the busy hour, when the channel is under-utilized, thus efficiently distributing the transmission requirements in time. More specifically, the state $|\phi^+\rangle$ of an ebit is given by the following Bell state:

$$|\phi^+\rangle = \frac{|00\rangle^{T_X R_X} + |11\rangle^{T_X R_X}}{\sqrt{2}}, \tag{12}$$

where T_X and R_X denotes the transmitter's and receiver's half of the ebit, respectively. Similar to the superdense coding protocol of [38], it is assumed that the receiver's half of the c ebits are transmitted over a noiseless quantum channel, while the transmitter's half of the c ebits together with the $(n-k-c)$ auxiliary qubits are used for encoding the intended k information qubits into n coded qubits. The resultant n-qubit codewords $|\overline{\psi}\rangle$ are transmitted over a noisy quantum channel. The receiver then combines his half of the c noiseless ebits with the received n-qubit noisy codewords $|\hat{\psi}\rangle$ to compute the syndrome, which is used for estimating the error pattern $\tilde{\mathcal{P}}$ incurred on the n-qubit transmitted codewords. The rest of the processing at the receiver is the same as that in Fig. 2.

The entangled state of Eq. (12) has unique commutativity properties, which assist us in transforming a set of non-Abelian generators into an Abelian set. The state $|\phi^+\rangle$ is stabilized by the operators $\mathbf{X}^{T_X}\mathbf{X}^{R_X}$ and $\mathbf{Z}^{T_X}\mathbf{Z}^{R_X}$, which commute with each other. Therefore, we have[10]:

$$[\mathbf{X}^{T_X}\mathbf{X}^{R_X}, \mathbf{Z}^{T_X}\mathbf{Z}^{R_X}] = 0. \tag{13}$$

However, local operators acting on either of the qubits anti-commute, i.e. we have:

$$\{\mathbf{X}^{T_X}, \mathbf{Z}^{T_X}\} = \{\mathbf{X}^{R_X}, \mathbf{Z}^{R_X}\} = 0. \tag{14}$$

Therefore, if we have two single qubit operators $\mathbf{X}^{T_X}$ and $\mathbf{Z}^{T_X}$, which anti-commute with each other, then we can resolve the anti-commutativity by entangling another qubit and choosing the local operators on this additional qubit such that the resultant two-qubit generators ($\mathbf{X}^{T_X}\mathbf{X}^{R_X}$ and $\mathbf{Z}^{T_X}\mathbf{Z}^{R_X}$ for this case) commute. This additional qubit constitutes the receiver half of the ebit. In other words, we entangle an additional qubit for the sake of ensuring that the resultant two-qubit operators have an even number of places with different non-identity operators, which in turn ensures commutativity.[11]

III. QUANTUM LDPC CODE DESIGNS

Analogous to classical LDPC codes, which belong to the family of linear block codes, QLDPC codes are inherently stabilizer codes, which may be characterized using an equivalent classical Parity Check Matrix (PCM) H of Eq. (5).

[9] Two qubits are said to be entangled if they cannot be decomposed into the tensor product of the constituent qubits. Consequently, a peculiar link exists between the two qubits such that measuring one qubit also collapses the other, despite their spatial separation [25].

[10] $[a, b]$ represents the commutative relation between a and b, while $\{a, b\}$ denotes the anti-commutative relation.

[11] For example, if $g_1 = \mathbf{XZI}$ and $g_2 = \mathbf{ZII}$, which anti-commute, then we can resolve the anti-commutativity by using an additional entangled qubit for extending the generators g_1 and g_2 to $g_1' = \mathbf{XZI|X}$ and $g_2' = \mathbf{ZII|Z}$, respectively, where the Pauli operators to the left of the vertical bar (|) act on the n-qubit codeword, while that to the right of the vertical bar acts on the receiver's half of the ebit.

More specifically, an $[n, k]$ QLDPC code having a coding rate of $R_Q = k/n$ is equivalent to a $(2n, n+k)$ binary LDPC code having a coding rate of $R_c = (n+k)/2n$. We may divide the QLDPC codes into three main categories on the basis of the general global structure of the associated PCM H, namely Calderbank-Shor-Steane (CSS) codes, non-CSS codes and Entanglement-Assisted (EA) codes, as summarized in Fig. 4. The CSS-type constructions may also be classified as dual-containing and as non-dual-containing codes. Let us now take a look at each of these categories individually.

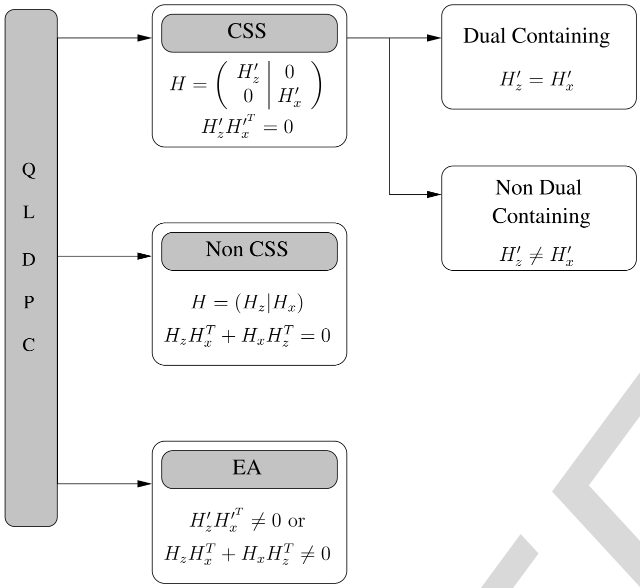

FIGURE 4. Classification of QLDPC codes.

A. CALDERBANK-SHOR-STEANE CODES

Ideally, any two classical binary LDPC codes, which meet the symplectic criterion, may be used for constructing a CSS-based QLDPC code. However, randomly choosing the constituent pair of classical codes is not feasible, because finding two sparse codes, which satisfy the stringent symplectic constraint, is highly unlikely. This motivated Postol [39] to conceive the first example of a CSS-based non-dual-containing QLDPC code from a small (15, 7) finite geometry based classical LDPC code in 2001. More specifically, in Postol's code, the PCM of a finite geometry based cyclic classical LDPC code constitutes the H'_z of Eq. (8), while H'_x is derived from H'_z, so that the symplectic criterion is satisfied, i.e. we have $H'_z H'^T_x = 0$. Since both the constituent PCMs, i.e. H'_z and H'_x, are cyclic, this facilitates the implementation of the encoder. However, Postol did not develop a generalized method for his proposed design, which could facilitate the construction of QLDPC codes from any arbitrary finite geometry based classical LDPC codes. This gap was filled by Mackay *et al.* in [29], where several systematic constructions were developed for the CSS-based QLDPC codes by restricting the designs to the dual-containing structure.

Before proceeding with the constructions of [29], let us take a look at the symplectic condition of Eq. (7) in the context of the dual-containing QLDPC codes. Recall from Section II that the symplectic criterion of Eq. (7) reduces to $H'_z H'^T_z = 0$ for the dual-containing QLDPC codes, which have $H'_x = H'^T_z$. This in turn implies that the PCM of a classical LDPC code may only be used for constructing a dual-containing QLDPC code if:

1) it has an even row weight; and
2) every pair of rows has an even number of overlapping 1's, which we may term as an 'even overlap'.

By contrast, good classical LDPC codes must have at most a single overlapping 1 between every pair of rows for the sake of avoiding length-4 cycles because short cycles of length-4 impair the performance of the associated decoding algorithm. Consequently, the 'even overlap' condition results in unavoidable cycles of length 4 in the resultant PCM, as depicted in Fig. 5 for a random binary PCM H'_z given by[12]:

$$H'_z = \begin{pmatrix} 1 & 0 & 1 & 1 \\ 1 & 1 & 1 & 0 \end{pmatrix}. \tag{15}$$

Furthermore, the constraint $H'_z H'^T_z = 0$ also implies that the code-space of the underlying classical code must contain its dual. Hence, the resultant code contains codewords having a weight equal to the row weight ρ. Therefore, the minimum distance of the classical dual-containing code is upper-bounded by ρ. Surprisingly, this upper-bound does not exist for quantum codes due to the degenerate nature of quantum errors. More specifically, the n-tuple channel error pattern acting on the codewords of a QSC, may be classified as:

1) **Detected Error Patterns:** These error patterns anti-commute with the stabilizers of the code, yielding a non-trivial syndrome.
2) **Harmful Undetected Error Patterns:** This class of error patterns commutes with the stabilizers. Consequently, these error patterns are harmful, because they map one valid codeword onto another; thus, corrupting the codeword without triggering a non-trivial syndrome. Harmful undetected error patterns are attributed to the small minimum distance of the code.

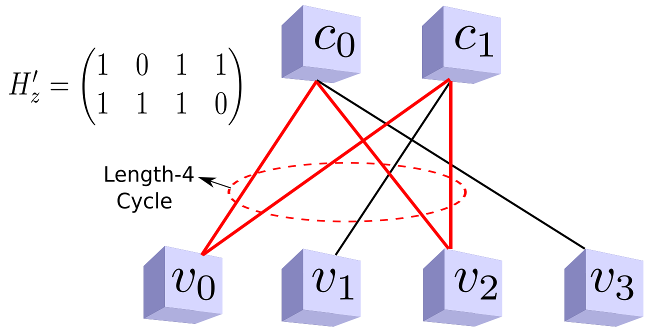

FIGURE 5. Tanner graph of H'_z. An 'even overlap' between the rows of H'_z results in a length-4 cycle.

[12]This is a random example for illustrating the impact of an even number of overlaps. The H'_z of Eq. (15) may not be a good classical code.

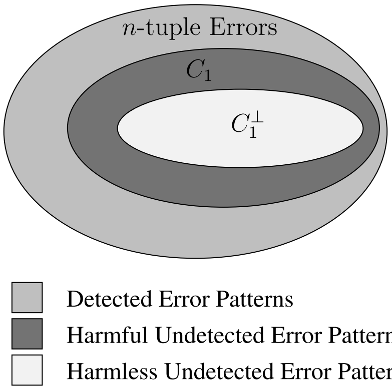

FIGURE 6. Error pattern classification for dual-containing CSS codes.

3) **Harmless Undetected Error Patterns:** This is a unique class of error patterns, which do not have a classical analogue. Similar to the 'harmful undetected error patterns', these error patterns also commute with the stabilizers, but they are harmless in the context of quantum codes. This is because these are the degenerate errors, which belong to the stabilizer group, and therefore do not corrupt the state of the valid codewords. More explicitly, for dual-containing CSS codes, the harmless undetected error patterns lie in the code-space of the dual code $C_1^{\perp}$, as depicted in Fig. 6. It must be mentioned here that although the harmless undetected errors do not affect the minimum distance of the resultant quantum code, they lead to the 'symmetric degeneracy error' in the iterative decoding procedure of QLDPC codes, which will be discussed in Section IV-C.

Bicycle codes, which were proposed by Mackay *et al.* in [29], marked the first major breakthrough towards the realization of CSS-based dual-containing quantum LDPC codes. The proposed code design relies on a semi-random/semi-structured construction, which satisfies the dual-containing constraint by deliberately imposing a global structure on the constituent PCM. A bicycle code having a row weight of ρ, a block length of n and $(n-k)$ stabilizers is constructed using a random sparse $n/2 \times n/2$ cyclic matrix C_m, which has a row weight of $\rho/2$. The non-zero entries in C_m can be chosen either randomly or using a difference set satisfying the property that every difference (modulo $n/2$) occurs at most once in the set. This matrix C_m is then used for constructing a base matrix H_0, which is a concatenation of C_m and its transpose, i.e. we have:

$$H_0 = \left(C_m, C_m^T\right). \tag{16}$$

Consequently, H_0 is a dual-containing code satisfying the 'even overlap' constraint, because every overlap that occurs in C_m may also be found in C_m^T. Furthermore, since H_0 is an $n/2 \times n$ matrix, the resultant dual-containing quantum LDPC code has a coding rate $R_Q = 0$ (or equivalently $R_c = 1/2$). To achieve a non-zero coding rate, k rows of H_0 are discarded, so that the column weights of the resultant $(n-k) \times n$ PCM H_z' are as uniform as possible. This code design offers flexibility in choosing the code parameters, i.e. ρ, n and k. However, the minimum distance of the resultant code is upper-bounded by ρ. This is because the discarded rows of H_0 are all codewords of weight ρ, which are not contained in the dual, and therefore contribute to the harmful undetected error patterns.

Mackay *et al.* also proposed unicycle codes in [29], which are derived from perfect difference sets.[13] The perfect difference set property implies that all pairs of rows of the PCM must have a single overlapping 1. Since we need an 'even overlap' to achieve a dual-containing structure, the PCM is extended by adding an extra column having all logical ones. Hence, every pair of rows in the resultant PCM have two overlapping 1's, which result in a single length-4 cycle between every pair of rows. Thus, an (n, k) PCM is transformed into a dual-containing $(n+1, k+1)$ PCM, which has a row weight of $(\rho+1)$ (where ρ is the row weight of the initial matrix and must be odd) and whose column weights are all ρ, except for the last 'all-one' column. Mackay *et al.* also suggested that the unique structure of unicycle codes may be exploited for avoiding the length-4 cycles during the decoding procedure [29]. More explicitly, a unicycle code may be viewed as a superposition of two codes, i.e. one having an 'all-zero' column at the end and the other having an 'all-one' column. For the sake of avoiding the short cycles, each of the two codes is decoded separately using the sum product algorithm [29]. If both decoders return a valid codeword, the codeword which has the maximum likelihood is chosen. Hence, an improved decoding procedure is conceived at the cost of an increased decoding complexity. Furthermore, the minimum distance of the unicycle codes constructed using difference sets is upper-bounded by the row weight, because the resultant code has codewords of weight ρ, which do not lie in the dual. Since the choice of n, k and ρ for perfect difference sets is limited, this design does not offer much flexibility in choosing the code parameters. By contrast, bicycle codes can be constructed from any arbitrary cyclic classical LDPC.

To extend the application of Mackay's unicycle codes to a wider range of code parameters, Aly [40] exploited the classical type-II Euclidean Geometry (EG) LDPC codes of [41]. Similar to the perfect difference sets, a classical type-II EG LDPC code having a PCM $H_{\text{EG-II}}$ has the unique characteristic that all pairs of rows have a single overlapping value of 1. Consequently, Aly suggested that the code characterized by

[13] A perfect difference set characterized on the additive group of size n has the unique property that every integer from 1 to $n-1$ may be expressed as a difference of two integers in the set (modulo n) in exactly one way. By contrast, in the plain difference sets, every difference occurs at most once, i.e. either it may not occur or will occur only once. For example, the set $\{1, 2, 4\}$ forms a perfect difference set for the group of size 7 because every integer from 1 to 6 can be expressed as the difference of two elements in the difference set, i.e. we have:

$$\begin{aligned}(1-2)\bmod 7 &= 6, \quad (1-4)\bmod 7 = 4, \quad (2-1)\bmod 7 = 1,\\ (2-4)\bmod 7 &= 5, \quad (4-1)\bmod 7 = 3, \quad (4-2)\bmod 7 = 2.\end{aligned}$$

an $(n-k) \times n$ matrix $H_{\text{EG-II}}$ may be converted into a dual-containing code in the following two ways:

1) If the row weight of $H_{\text{EG-II}}$ is odd, then similar to the unicycle codes, an 'all-one' column $\mathbf{1}$ is appended to $H_{\text{EG-II}}$, i.e. we have:

$$H'_z = (H_{\text{EG-II}}|\mathbf{1}). \tag{17}$$

2) If the row weight of $H_{\text{EG-II}}$ is even, then $\mathbf{1}$ is appended to $H_{\text{EG-II}}$ for the sake of ensuring an 'even overlap', while an identity matrix $\mathbf{I}$ of size $(n-k) \times (n-k)$ is appended to make the row weight even, i.e. we have:

$$H'_z = (H_{\text{EG-II}}|\mathbf{1}|\mathbf{I}). \tag{18}$$

The resultant codes offer beneficial high coding rates. However, they have an upper-bounded minimum distance of at least $(\gamma + 1)$, where γ denotes the column weight.

Unicycle code construction was further explored by Djordjevic [42] for designing Quasi-Cyclic (QC) high-rate dual-containing QLDPC codes from the Balanced Incomplete Block Design (BIBD) based classical LDPC codes [43], [44], which have a minimum distance of at least $(\gamma + 1)$, where γ denotes the column weight. More specifically, the BIBD[14] is characterized by the parameter λ. A BIBD-based LDPC code has exactly λ overlaps between every pair of rows. Since good classical LDPC codes must have at most a single row overlap, λ is set to 1 for designing classical LDPC codes with a girth of at least 6. Consequently, analogous to the perfect difference set based classical LDPC codes, each pair of rows has a single overlapping value of 1, which can be made even by imposing the unicycle code structure on the PCM. Djordjevic also designed dual-containing LDPC codes by using BIBDs associated with an even λ. Unfortunately, the even λ based QLDPC codes failed to outperform the unicycle based BIBD constructions [42].

Since all the aforementioned dual-containing constructions resulted in an upper-bounded minimum distance, the quest for the construction of unbounded QLDPC codes continued. Pursuing this objective, another non-trivial class of dual-containing QLDPC codes was proposed by Mackay *et al.* in [45], which was derived from Cayley graphs. These codes were further investigated by Couvreur *et al.* in [46] and [47], where it was formally shown that the lower bound on the minimum distance of the resultant code is a logarithmic function of the code length, thus the minimum distance can be improved by extending the codeword (or block) length, albeit again, only logarithmically. However, this is achieved at the cost of an increased decoding complexity imposed by the escalating row weight, which also increases logarithmically with the block length. Furthermore, Cayley graph based designs may be viewed as a special class of the topological codes [48]–[50],[15] which are already known to have growing minimum distances.

Let us recall that the dual-containing QLDPC codes have unavoidable short cycles, which impair the performance of the decoding algorithm. Hence, even if dual-containing QLDPC codes having an unbounded minimum distance are designed, they are unlikely to surpass the performance of their non-dual-containing counterparts. Therefore, in the midst of these activities, Lou and Garcia-Frias [55], [56] rekindled the interest in CSS-based non-dual-containing QLDPC codes by invoking the classical Low Density Generator Matrix (LDGM) codes for code construction. More specifically, since both the generator matrix and the PCM of an LDGM code are sparse, they can be used as the components of a CSS code. Let $\tilde{G}$ and $\tilde{H}$ be the generator matrix and PCM, respectively, of an (n, k) LDGM code. Then the resultant CSS code may be formulated as follows:

$$H = \begin{pmatrix} \tilde{H} & \mathbf{0} \\ \mathbf{0} & \tilde{G} \end{pmatrix}. \tag{19}$$

Since $\tilde{H}$ is an $(n-k) \times n$ matrix, while $\tilde{G}$ is a $k \times n$ matrix, the resultant PCM H is an $n \times 2n$ matrix. Consequently, the corresponding QLDPC code has a coding rate of zero. Lou and Garcia-Frias [55], [56] suggested that this may be avoided by applying linear row operations both to $\tilde{G}$ as well as to $\tilde{H}$ for the sake of reducing their number of rows. Unfortunately, this row-reduction may in turn create short cycles in the resultant PCM. For the sake of avoiding the adverse impact of these short cycles, Lou and Garcia-Frias [55], [56] also conceived a modified Tanner graph, which requires code doping [57] for pushing the iterative decoding process towards convergence. Hence, an improved performance is achieved at the cost of an increased decoding complexity.

Unfortunately, the constituent codes of all the aforementioned CSS constructions, both those of the dual-containing as well as of the non-dual-containing codes, suffer from the presence of length-4 cycles. To dispense with these short cycles, Hagiwara and Imai [58], [59] conceived a unique class of non-dual-containing QC-QLDPC codes, which have a girth of at least 6. More specifically, let us consider a circulant matrix T having a size of $LP/2 \times LP/2$, $\rho = L/2$ and $\gamma = L$, which is given by [59]:

$$T = \begin{pmatrix} t_0 & t_1 & \ldots & t_{L/2-1} \\ t_{L/2-1} & t_0 & \ldots & t_{L/2-2} \\ \vdots & & & \vdots \\ t_1 & t_2 & \ldots & t_0 \end{pmatrix}, \tag{20}$$

[14] $\text{BIBD}(v, b, r, k, \lambda)$ distributes all the v elements (or points) of a set V into b subsets (or blocks) of size k such that,

- each pair of elements occurs in exactly λ of the blocks,
- every element occurs in exactly r blocks, and
- the number of elements in each block k is small as compared to the size v of set V; thus, giving it the name "incomplete."

Let us consider a set V of seven numbers, which is given by $V = \{1, 2, 3, 4, 5, 6, 7\}$. Then, the blocks $\{1, 2, 4\}$, $\{2, 6, 5\}$, $\{3, 4, 6\}$, $\{4, 5, 7\}$, $\{1, 5, 6\}$, $\{2, 6, 7\}$ and $\{1, 3, 7\}$ constitute the $\text{BIBD}(7, 7, 3, 3, 1)$ since there are 7 elements (v) in the set V which are distributed among 7 blocks (b), each element appears in 3 blocks (r), each block has 3 elements (k) and each pair of elements occur in 1 block (λ).

[15] The family of topological codes, e.g. [48]–[54], is beyond the scope of this work.

where t_i denotes the index of the circulant permutation matrix[16] of size P and $t_i \in [P_\infty] := \{0, 1, \ldots, P-1\} \cup \{\infty\}$. Hagiwara *et al.* have shown that H'_z and H'_x derived from the matrix T of Eq. (20) satisfy the symplectic criterion, if they have the form:

$$H'_z = (T_1, T_2) \text{ and } H'_x = \left(-T_2^T, -T_1^T\right). \tag{21}$$

Furthermore, since row deletion does not perturb the symplectic criterion, rows may be deleted from H'_z and H'_x in order to achieve the desired coding rate. For the sake of ensuring a girth of 6, Hagiwara *et al.* relied upon algebraic combinatorics for designing the constituent circulant matrices T_1 and T_2, so that all the rows of H'_z as well as of H'_x have at most a single overlap. The bicycle codes of [29] may be viewed as a special case of this construction, i.e. when $P = 1$ and $T_2 = T_1^T$. Unfortunately, the resultant codes failed to outperform MacKay's bicycle codes [29] and their minimum distance is upper-bounded by the row weight.

Among all the dual-containing codes discussed above, Mackay's bicycle construction [29] offers the best performance at an affordable decoding complexity. However, the resultant performance is still not on par with that of the classical LDPC codes. For example, the rate-$1/4$ bicycle code of [29], having $n = 19,014$, operates within about 5.5 dB of the Hashing limit at a Word Error Rate (WER) of 10^{-3}. Furthermore, all the aforementioned codes have an upper-bounded minimum distance except for the Cayley graph based designs. In the quest for increasing the minimum distance and hence to approach the capacity, Hagiwara *et al.* extended the QC design of [58] and [59] to Spatially-Coupled (SC) codes in [60], which outperformed their corresponding 'non-coupled' counterparts at the cost of a small coding rate loss. However, the performance still remained relatively far from the capacity. More specifically, the SC QC-QLDPC of [60], having a coding rate of 0.49 and a length of $n = 1,81,000$, operates within about 3.8 dB of the Hashing limit at a WER of 10^{-3}. Kasai *et al.* further contributed to these developments by deriving non-binary QC-QLDPC codes in [61] and [62] from the design of [58] and [59]. The resultant codes outperformed their binary counterparts at the cost of an increased decoding complexity. A rate-$1/2$ code, having a length of $n = 20,560$ and a Galois field of GF(2^{10}), was shown to operate within about 1.9 dB of the Hashing limit at a WER of 10^{-3}. The SC codes were further investigated by Andriyanova *et al.* in [63], where the constituent codes were derived from the classical LDGM codes as in [55] and [56]. Analogous to the EA quantum codes, Andriyanova *et al.* assumed that some qubits are transmitted over a noiseless channel. Consequently, the resultant rate-1/4 LDGM-based SC-QLDPC codes, having a length of $n = 76,800$, succeeded in operating within about 1.7 dB of the Hashing limit at a WER of 10^{-3}. The assumption of having noiseless qubits was later eliminated in [64], whereby these qubits were protected by the error reducing Quantum Turbo Code (QTC) of [64], which resulted in a modest coding rate loss and in a moderately increased complexity for the overall code. It was shown that the performance of the resultant rate-$1/2$ QTC-assisted LDGM-based SC-QLDPC code, having a length of $n = 8,21,760$, is within about 0.7 dB of the Hashing limit at a WER of 10^{-3}. Fig. 7 compares the achievable performance of the aforementioned codes, namely of the 'bicycle' code of [29], 'SC QC-QLDPC' code of [60], 'non-binary QC-QLDPC' code of [61] and [62], 'LDGM-based SC-QLDPC' code of [63] and the 'QTC-assisted LDGM-based SC-QLDPC' code of [64], at a WER of 10^{-3}, which is benchmarked against the Hashing bound.

All the main contributions pertaining to CSS-based QLDPC codes are summarized in Fig. 8.

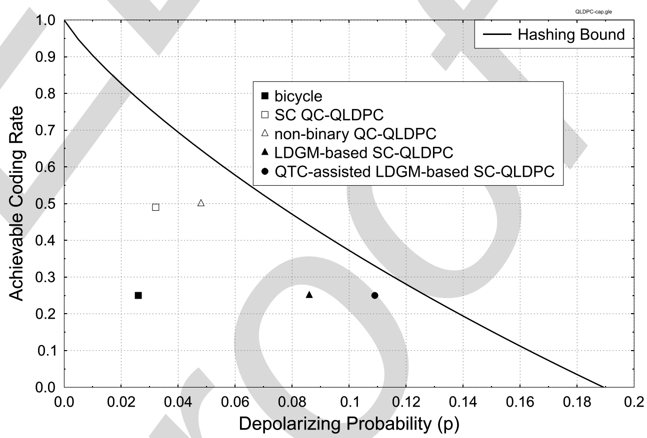

FIGURE 7. **Achievable performance at a WER of 10^{-3} benchmarked against the Hashing bound for the 'bicycle' code ($R = 0.25$, $n = 19,014$) of [29], 'SC QC-QLDPC' code ($R = 0.49$, $n = 1,81,000$) of [60], 'non-binary QC-QLDPC' code ($R = 0.5$, $n = 20,560$, GF(2^{10})) of [61] and [62], 'LDGM-based SC-QLDPC' code ($R = 0.25$, $n = 76,800$) of [63] and the 'QTC-assisted LDGM-based SC-QLDPC' code ($R = 0.25$, $n = 8,21,760$) of [64].**

B. NON-CSS CODES

Non-CSS stabilizer codes have the potential of exploiting any redundancy more efficiently than their CSS-based counterparts. For example, a CSS-based block code requires a block length of 7 qubits to correct a single bit-flip or phase-flip [31], while only 5 qubits are required for a non-CSS block code [75]. Consequently, Camara *et al.* [65], [66] proposed the construction of non-CSS (also called unrestricted) QLDPC codes. In contrast to most of the aforementioned dual-containing constructions, which satisfy the symplectic criterion in their global code

[16] A circulant permutation matrix $I(1)$ of size P is given by:

$$I(1) = \begin{pmatrix} 0 & 1 & 0 & \ldots & 0 \\ 0 & 0 & 1 & \ldots & 0 \\ 0 & 0 & 0 & \ldots & 0 \\ \vdots & & & & \vdots \\ 1 & 0 & 0 & \ldots & 0 \end{pmatrix}.$$

More explicitly, $I(1)$ is a $P \times P$ identity matrix shifted to the right by one position. Therefore, $I(x)$ may be defined as a $P \times P$ identity matrix shifted to the right by x positions, where x is known as the index of the permutation matrix. Moreover, $x = 0$ defines an unshifted identity matrix, while $x = \infty$ is specially used to denote a zero matrix of size $P \times P$.

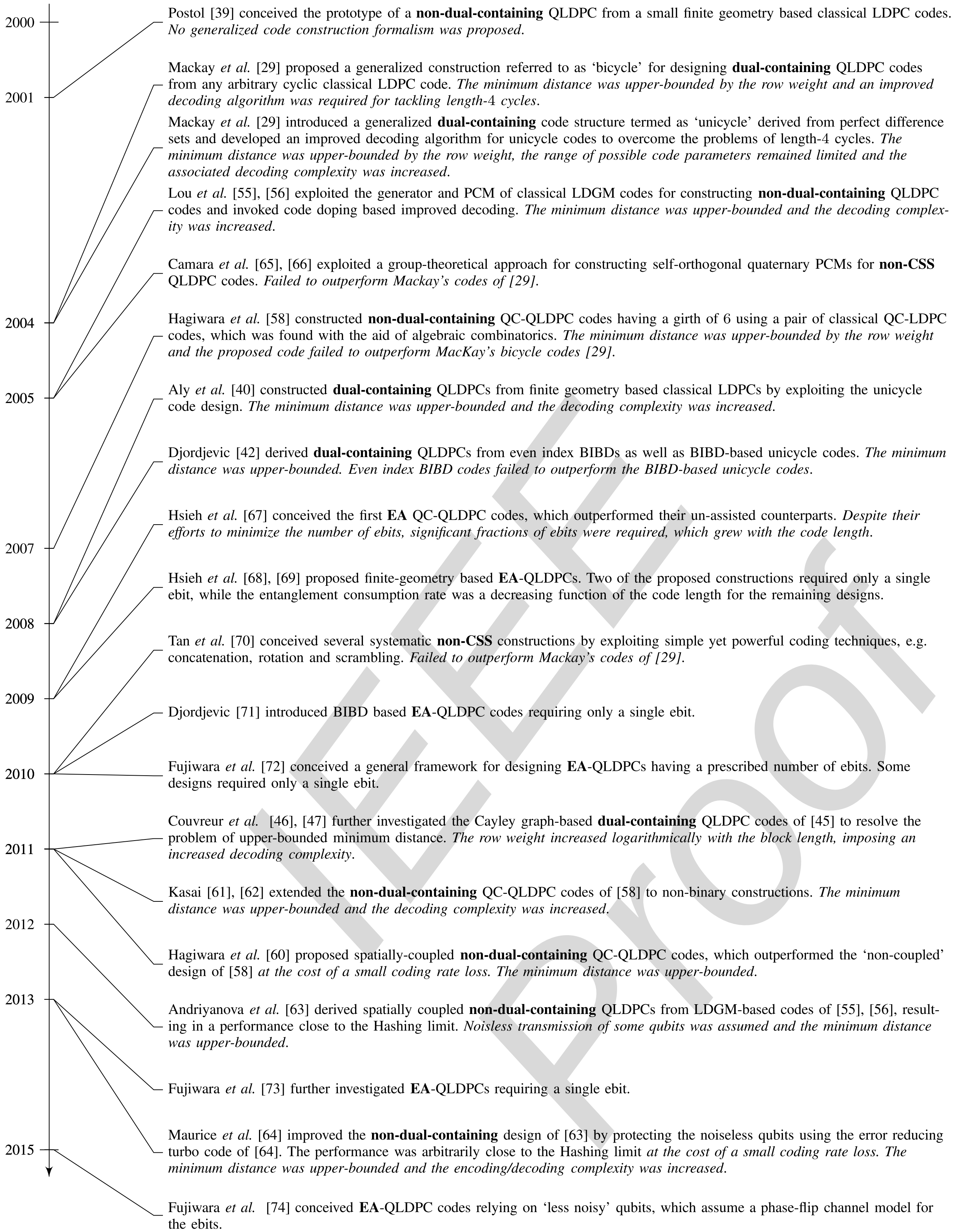

FIGURE 8. Major contributions to the development of QLDPC codes. The ‘code type’ for each contribution is highlighted in bold, while the associated ‘demerits’ are marked in *italics*.

structure, the design conceived by Camara *et al.* aims at building the symplectic constraint into the local code structure. More specifically, since the PCM of a classical quaternary LDPC code can be mapped onto the generators of a QSC based on Eq. (9), Camara *et al.* developed a group theoretical approach for constructing self-orthogonal quaternary LDPC codes satisfying the symplectic criterion of Eq. (11). It was found that the Tanner graph of the resultant self-orthogonal quaternary PCM has cycles of length 4. However, these short cycles are imposed by the commutativity constraint. More specifically, every column of a quaternary PCM must contain at least two different non-zero entries, i.e Pauli-**X**, Pauli-**Z**, or Pauli-**Y**, so that it can correct both phase-flips as well as bit-flips occurring on that qubit. On the other hand, any two rows of the PCM must have an even number of positions with different non-zero elements (or non-Identity Pauli operators). For example, let us consider a weight-2 column of a PCM, which is involved in two rows with a value of 1 and ω, respectively. Now to meet the commutativity constraint, these two rows must have another overlapping column having different non-zero entries; thus, creating cycles of length-4. Intuitively, these short cycles are also present in the PCM H of the CSS codes, when they are viewed in the quaternary domain. In fact, these cycles are excessive in the dual-containing CSS codes, which also have the additional cycles resulting from the dual-containing constraint.[17] The proposed non-CSS QLDPC codes of [65] and [66] outperformed the bicycle codes in the waterfall region of their performance curve, while yielding a higher error floor due to their small minimum distance. It is expected that this non-CSS construction may have an unbounded minimum distance, thus yielding lower error floors, when the block length is sufficiently large. However, this was not explicitly proven in [65] and [66].

Pursuing the same line of research, Tan and Li [70] were the first researchers to design the constituent PCMs H_z and H_x of a non-CSS code by invoking classical binary codes. More specifically, they conceived several systematic constructions for non-CSS QLDPC codes, which imposed both global as well as local structures on the underlying binary codes for the sake of satisfying the symplectic criterion. This is achieved by exploiting simple yet powerful coding techniques, which include concatenation, rotation and scrambling. The designed codes exhibit a better performance than the non-CSS codes of [65] and [66]. However, they still failed to outperform Mackay's codes of [29]. In conclusion, the major milestones achieved in the domain of non-CSS QLDPC codes are summarized in Fig. 8.

C. ENTANGLEMENT-ASSISTED QLDPC CODES

Efficient classical LDPC codes exist, which are known to approach the Shannon capacity for a large block size. For example, the optimized $1/2$-rate classical LDPC code of [76] operates within 0.13 dB of the capacity limit for transmission over an Additive White Gaussian Noise (AWGN) channel at a Bit Error Rate (BER) of 10^{-6} using a code length of 10^6. More specifically, the turbo cliff of this LDPC code is merely 0.06 dB away from the Shannon capacity. This inspired researchers to achieve a comparable performance for QLDPCs. Unfortunately, the symplectic criterion, or more specifically the commutativity requirement of the stabilizers, limits the direct application of such efficient classical codes in the quantum domain. As discussed in Sections III-A and III-B, only a limited class of classical codes, which conform to stringent local or global structural constraints, may be used as the constituents of a quantum code. This obstacle may be overcome by exploiting the EA quantum code designs of [35]–[37], which assist us in importing any classical code into the quantum domain. However, the pre-shared noiseless entangled qubits (ebits) of an EA code constitute a valuable resource, because maintaining a noiseless entangled state is not a trivial task. Consequently, a practically realizable code design should aim for minimizing the number of pre-shared noiseless ebits.

The first EA-QLDPC codes were conceived by Hsieh *et al.* in [67], whereby EA CSS-based QC-QLDPC codes were designed from their classical counterparts. Hsieh *et al.* chose the constituent circulant matrices of the classical QC code by ensuring that the number of ebits required is minimized. Despite their efforts, a significant number of these ebits was required, which grew with the code length. More importantly, these designs supported the conjecture that the high efficiency of EA codes should be attributed to the large fractions of pre-shared ebits. On a positive note, since the EA quantum codes of [67] shared the same attributes as the classical parent code, especially in terms of the girth and the minimum distance, these EA-QLDPC codes outperformed the state-of-the-art unassisted QLDPC codes. Working further in the direction of minimizing the number of pre-shared ebits, in [68] and [69] Hsieh *et al.* conceived finite-geometry based EA-QLDPCs, whose 'entanglement consumption rate' decreases with the code length. Furthermore, two of these constructions required only a single ebit regardless of the code length; thus dispensing with the then prevailing apprehensions surrounding the family of EA-codes. It must be emphasized here that the proposed design does not impose any restrictions on the underlying finite geometry based classical LDPC codes of [41]. A more general framework conceived for designing the EA-QLDPCs, having a prescribed number of ebits, was presented in [72], which was derived from combinatorial design theory. Some of these designs required only a single ebit, despite having a high performance, a high coding rate and a low complexity. The necessary and sufficient conditions for designing single-ebit based EA-QLDPCs were further investigated in [73]. Moreover, BIBD based EA-QLDPC codes requiring only a single ebit were also identified in [71]. Recently, Fujiwara [77] introduced the notion of quantum codes relying on 'less noisy' (or 'reliable') qubits. More explicitly, unlike the EA formalism, which requires completely noiseless ebits, the framework of [77] assumes that these auxiliary qubits are subjected to a phase-flip channel,

[17] This is further discussed in Section IV-C.

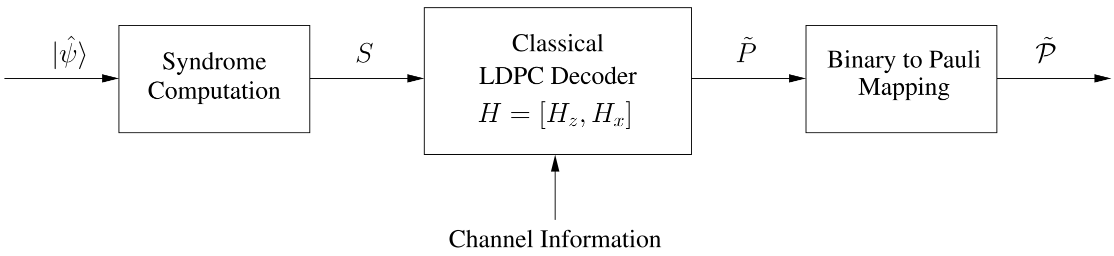

FIGURE 9. **General schematic of a syndrome-based decoder for QLDPC codes.**

which is a more realistic noise model. In this spirit, Fujiwara *et al.* [74] conceived QLDPC codes relying on 'less noisy' qubits. The major contributions made in the domain of EA-QLDPC codes are summarized in Fig. 8.

IV. ITERATIVE DECODING OF QUANTUM LDPC CODES

Analogous to the classical LDPC codes, QLDPC codes invoke the classic Belief Propagation (BP) based decoding, also referred to as the Sum-Product Algorithm (SPA), which operates over the Tanner graph of the corresponding PCM. However, let us recall from Section II that qubits collapse upon measurement. Therefore, the syndrome-based version [78] of the classic codeword decoding has to be used for QLDPC codes. The underlying BP can be implemented both in the binary as well as in the quaternary domain, which are discussed in Sections IV-A and IV-B, respectively.

A. BINARY DECODING

A quantum depolarizing channel characterized by the depolarizing probability p is isomorphic to two independent Binary Symmetric Channels (BSCs) [29], i.e. one for phase-flips and the other for bit-flips, each having a cross-over probability of $2p/3$. More explicitly, based on the Pauli-to-binary isomorphism encapsulated in Eq. (4), a Pauli error $\mathcal{P} \in \mathcal{G}_n$ experienced by an n-qubit block transmitted over a depolarizing channel can be modeled by an effective error-vector P, which is a binary vector of length $2n$. The effective error P may be represented as $P = (P_z, P_x)$, where both P_z and P_x are n-bit long and represent $\mathbf{Z}$ and $\mathbf{X}$ errors, respectively. This implies that an $\mathbf{X}$ error imposed on the tth qubit will yield a 0 and a 1 at the tth and $(n+t)$th index of P, respectively. Similarly, a $\mathbf{Z}$ error imposed on the tth qubit will give a 1 and a 0 at the tth and $(n+t)$th index of P, respectively, while a Y error on the tth qubit will result in a 1 at both the 1st as well as $(n+t)$th index of P. Since a depolarizing channel characterized by the probability p incurs $\mathbf{X}$, $\mathbf{Y}$ and $\mathbf{Z}$ errors with an equal probability of $p/3$, the effective error-vector P reduces to two BSCs having a crossover probability of $2p/3$, where we have one channel for the $\mathbf{Z}$ errors and the other for the $\mathbf{X}$ errors.

Based on the aforementioned simplified notion, which ignores the correlation between the $\mathbf{X}$ and $\mathbf{Z}$ errors, QLDPC codes can be decoded by running the syndrome-based BP over the Tanner graph of the equivalent binary code having $H = (H_z|H_x)$ [70]. More explicitly, let S be the observed syndrome sequence, which is given by the symplectic product of H and P, as formulated below:

$$S = H \star P^T = H_z P_x^T + H_x P_z^T. \tag{22}$$

The observed syndrome S of Eq. (22) is fed to a classical syndrome-based LDPC decoder to estimate the most likely inflicted channel error $\tilde{P}$, as depicted in Fig. 9. For an H of size $m \times 2n$, where we have $m = (n-k)$, the resultant estimated error vector $\tilde{P}$ is of length $2n$, whose first n bits are for the estimated phase errors $\tilde{P}_z$, while the other n bits indicate the estimated bit errors $\tilde{P}_x$. Finally, the $2n$-bit binary vector is mapped onto the n-qubit Pauli error $\tilde{\mathcal{P}}$ based on the mapping encapsulated in Eq. (4). More explicitly, the tth and $(n+t)$th value of $\tilde{P}$ are combined based on Eq. (4) to estimate the error inflicted on the tth qubit.

For CSS codes, we have $H_z = \begin{pmatrix} H'_z \\ \mathbf{0} \end{pmatrix}$ and $H_x = \begin{pmatrix} \mathbf{0} \\ H'_x \end{pmatrix}$.

Consequently, the Tanner graph of the matrix H consists of two independent Tanner graphs corresponding to the matrices H'_z and H'_x. This in turn implies that $\mathbf{X}$ and $\mathbf{Z}$ errors can be decoded independently using the matrices H'_z and H'_x, respectively [29]. Hence, the Qubit Error Rate (QBER) of a CSS QLDPC code may be approximated by the sum of the BER of the constituent classical codes. More explicitly, if p_e^x and p_e^z are the classical BERs for H'_z and H'_x, respectively, then the overall QBER is equivalent to $(p_e^x + p_e^z - p_e^x p_e^z) \approx (p_e^x + p_e^z)$, which reduces to $2p_e^z$ for a dual-containing CSS code having $H'_x = H'_z$.

For a binary $m \times 2n$ LDPC matrix H, the classical LDPC decoder of Fig. 9 aims for finding the most likely error P of length $2n$ given the observed syndrome S, i.e. we have:

$$\tilde{P} = \underset{P \in (\mathbb{F}_2)^{2n}}{\operatorname{argmax}} \mathrm{P}(P|S), \tag{23}$$

where $\mathrm{P}(P|S)$ is the probability of experiencing the error $P \in (\mathbb{F}_2)^{2n}$ imposed on the transmitted codewords, given that the syndrome of the received qubits $|\hat{\psi}\rangle$ is $S \in (\mathbb{F}_2)^m$. Unfortunately, Eq. (23) defines an NP-complete problem [79]. A sub-optimal algorithm for solving Eq. (23) is constituted by the classic BP, which finds the element-wise optimum value rather than the global optimum. More explicitly, for $P = (P_0, P_1, \ldots, P_t, \ldots, P_{2n-1})$, BP finds P_t such that:

$$\tilde{P}_t = \underset{P_t \in \mathbb{F}_2}{\operatorname{argmax}} \mathrm{P}(P_t|S), \tag{24}$$

where $P(P_t|S)$ is the marginalized probability of the tth bit. The BP operates by exchanging messages over the Tanner graph of H having check nodes c_i for $i \in \{0, m-1\}$ and variable nodes v_t for $t \in \{0, 2n-1\}$. The messages sent by the ith check node c_i to the tth variable node are denoted by $m^{P_t}_{c_i \to v_t}$, while the messages directed from the tth variable node to the ith check node are given by $m^{P_t}_{v_t \to c_i}$, where P_t is the error imposed on the tth variable node. The overall syndrome-based message exchange procedure is summarized in Algorithm 1, which proceeds as follows [78]:

- **Initialization:** The algorithm begins by initializing the messages $m^{P_t}_{v_t \to c_i}$ according to the channel model $P_{ch}(P_t)$. For a BSC having a crossover probability of $2p/3$, we have:

$$\begin{aligned} m^0_{v_t \to c_i} &= 1 - 2p/3, \\ m^1_{v_t \to c_i} &= 2p/3. \end{aligned} \tag{25}$$

- **Horizontal message exchange:** Let $V(c_i)$ be the set of variable nodes connected to the check node c_i, i.e. $V(c_i) \equiv \{v_t : H_{it} = 1\}$, and $V(c_i) \setminus v_t$ be the set $V(c_i)$ excluding the variable node v_t. As depicted in Fig. 10a, in this step the algorithm runs through the rows of H (checks) and computes the message $m^{P_t}_{c_i \to v_t}$ for each $v_t \in V(c_i)$ and $P_t \in \mathbb{F}_2$. The message $m^a_{c_i \to v_t}$ represents the probability that the syndrome value observed for the check c_i is S_i given that the tth variable node has the error $(P_t = a)$, where $a \in \{0, 1\}$. This can be mathematically formulated as:

$$m^a_{c_i \to v_t} = K \sum_{P:P_t=a} P(S_i|P) \prod_{v_{t'} \in V(c_i)\setminus v_t} m^{P_{t'}}_{v_{t'} \to c_i}, \tag{26}$$

  where K is the normalization constant invoked for ensuring $\sum_{a\in\{0,1\}} m^a_{c_i \to v_t} = 1$, while $P(S_i|P)$ is a binary function, which is equal to 1 only when the check c_i is satisfied, i.e. when the value of the check node c_i computed using the error vector P matches the measured syndrome value S_i, otherwise it is 0. Furthermore, according to Eq. (26), the messages $m^a_{c_i \to v_t}$ destined for the tth variable node do not take into account the messages flowing in the opposite direction along the same edge, i.e. $m^a_{v_t \to c_i}$. Consequently, $m^a_{c_i \to v_t}$ only contains the new information gleaned from the messages sent by the other variable nodes and it is therefore termed as being '*extrinsic*'. This ensures that the successive iterations of this iterative algorithm are independent.

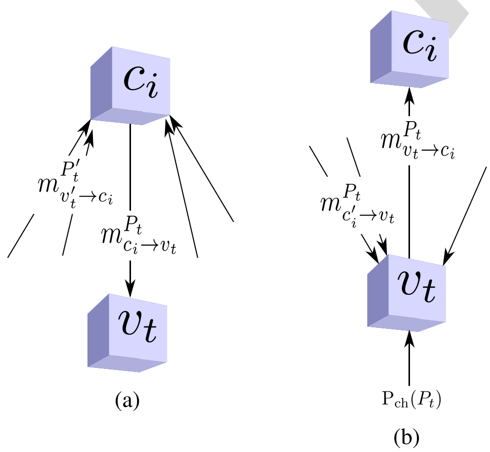

FIGURE 10. Belief Propagation (BP) algorithm. Check nodes and variable nodes are denoted by c_i and v_t, respectively. (a) Horizontal message exchange. (b) Vertical message exchange.

- **Vertical message exchange:** Let $C(v_t)$ be the set of check nodes connected to the variable node v_t, i.e. $C(v_t) \equiv \{c_i : H_{it} = 1\}$, and $C(v_t) \setminus c_i$ be the set $C(v_t)$ excluding the check node c_i. As shown in Fig. 10b, for each column of H (hence called 'vertical'), the BP computes the message $m^{P_t}_{v_t \to c_i}$ for all $c_i \in V(v_t)$ and $P_t \in \mathbb{F}_2$. More explicitly, the messages $m^a_{v_t \to c_i}$ are computed by evaluating the product of the channel information $P_{ch}(P_t = a)$ and the messages $m^a_{c_{i'} \to v_t}$ flowing into the variable node v_t along all the edges connected to it, but excluding $m^a_{c_i \to v_t}$, which is received along the same edge. Hence, the extrinsic message is computed as:

$$m^a_{v_t \to c_i} = K P_{ch}(P_t = a) \prod_{c_{i'} \in C(v_t)\setminus c_i} m^a_{c_{i'} \to v_t}, \tag{27}$$

  where k is the normalization constant, which ensures that $\sum_{a\in\{0,1\}} m^a_{v_t \to c_i} = 1$.
- **Element-wise marginal probability:** Finally, the element-wise marginal probability $P(P_t|S)$ for $P_t \in \mathbb{F}_2$ is calculated as follows:

$$P(P_t = a|S) = K P_{ch}(P_t = a) \prod_{c_i \in C(v_t)} m^a_{c_i \to v_t}, \tag{28}$$

  which takes into account all the messages flowing into the variable node v_t.
- **Hard decision & syndrome check:** As previously portrayed in Eq. (24), a hard decision is made by finding the most likely error $\tilde{P}_t$, which maximizes the marginal probability computed in Eq. (28). Based on the estimated error vector $\tilde{P}$, the syndrome $\tilde{S} = H(\tilde{P}_x : \tilde{P}_z)^T$ is computed. If the syndrome $\tilde{S}$ of the estimated error $\tilde{P}$ is the same as the observed syndrome S, the process halts, indicating that the correct solution is found. Otherwise, the algorithm repeats itself from the horizontal message exchange step onwards. This iterative procedure continues, until either $\tilde{S} = S$ or the maximum number of iterations $\mathtt{I}_{\max}$ is reached.

B. NON-BINARY DECODING

Based on the Pauli-to-GF(4) formalism of Eq. (9), QLDPC codes can be decoded by invoking the non-binary BP, which takes into account the correlation between the phase-flips and bit-flips. The syndrome-based non-binary BP is similar to the binary BP of Algorithm 1, with the following two major modifications:

- Non-binary BP exploits the depolarizing channel model, which does not ignore the correlation between the bit and

Algorithm 1 Syndrome-Based BP

Set $P_{\text{ch}}(0) \leftarrow (1-2p/3)$ and $P_{\text{ch}}(1) \leftarrow 2p/3$.
Initialize $m^a_{v_t \to c_i} \leftarrow P_{\text{ch}}(a), \forall\, v_t, c_i \in C(v_t)$ and $a \in \{0,1\}$.
for iter $\leftarrow$ 1 to $\mathcal{I}_{\max}$ **do**
  for all $i \in \{0, (m-1)\}$, $v_t \in V(c_i)$ and $a \in \{0,1\}$ **do**
    $m^a_{c_i \to v_t} \leftarrow k \sum_{P:P_t=a} \mathrm{P}(S_i|P) \prod_{v_{t'} \in V(c_i)\setminus v_t} m^{P_{t'}}_{v_{t'} \to c_i}$.
  end for
  for $t \leftarrow 0$ to $(2n-1)$ **do**
    for all $c_i \in C(v_t)$ and $a \in \{0,1\}$ **do**
      $m^a_{v_t \to c_i} \leftarrow k P_{\text{ch}}(P_t = a) \prod_{c_{i'} \in C(v_t)\setminus c_i} m^a_{c_{i'} \to v_t}$.
    end for
    for all $a \in \{0,1\}$ **do**
      $\mathrm{P}(P_t = a|S) \leftarrow k P_{\text{ch}}(P_t = a) \prod_{c_i \in C(v_t)} m^a_{c_i \to v_t}$.
    end for
    $\tilde{P}_t \leftarrow \arg\max_{P_t \in \mathbb{F}_2} \mathrm{P}(P_t|S)$.
  end for
  $\tilde{S} \leftarrow H(\tilde{P}_x : \tilde{P}_z)^T$.
  if $(\tilde{S} = S)$ **then**
    return $\tilde{P}$.
  end if
end for

phase errors. The equivalent 4-ary channel model has the following probability distribution:

$$\mathbf{P}_{\text{ch}}\left(\hat{P}_t = \hat{a}\right) = \begin{cases} 1-p, & \text{if } \hat{a} = 0 \\ p/3, & \text{if } \hat{a} \in \{1, \omega, \overline{\omega}\}, \end{cases} \tag{29}$$

where we have $\hat{P} = \left(\hat{P}_0, \hat{P}_1, \ldots, \hat{P}_t, \ldots, \hat{P}_{n-1}\right)$ and $\hat{P}_t$ denotes the error inflicted on the tth qubit.

- The syndrome S_i, which was computed as $H_i(P_x : P_z)^T$ in the binary scenario, is now given by the trace inner product of $\hat{H}_i$ and $\hat{P}$ (see Eq. (11)):

$$S_i = \mathrm{Tr}(\hat{H}_i \cdot \hat{P}), \tag{30}$$

where $\hat{H}_i$ is the ith row of H in GF(4) and $i \in \{0, m-1\}$. As compared to the binary BP, non-binary decoding imposes an increased complexity, specifically on the horizontal message exchange step. More explicitly, since the summation in Eq. (26) runs for all possible error sequences $\{\hat{P} : \hat{P}_t = \hat{a}\}$, which yield the syndrome S_i for the ith check node, the complexity increases both with the row weight as well as with the dimensionality of the Galois field. For classical non-binary LDPC codes, this increased complexity is alleviated by invoking the Fast Fourier Transform (FFT) based decoding of [80], which can be conveniently adapted to the syndrome-based decoding of QLDPC codes.

Based on the notion of the trace inner product of Eq. (11), Eq. (30) can be expanded as:

$$S_i = \mathrm{Tr}(\hat{S}_i) = \mathrm{Tr}\left(\sum_{t \in V(c_i)} \hat{H}_{it} \times \overline{\hat{P}}_t\right), \tag{31}$$

where we have $\hat{S}_i \in \{0, 1, \omega, \overline{\omega}\}$, which can also be expressed as:

$$\hat{S}_i = \hat{H}_{it} \times \overline{\hat{P}}_t + \sum_{t' \in V(c_i)\setminus v_t} \hat{H}_{it'} \times \overline{\hat{P}}_{t'}. \tag{32}$$

Unlike in the binary scenario, where we have $H_{it} \in \{0,1\}$, here we have $\hat{H}_{it} \in \{1, \omega, \overline{\omega}\}$ in Eq. (32). Therefore, given the messages $m^{\hat{a}}_{c_i \to v_t}$ and $m^{\hat{a}}_{v_t \to c_i}$ exchanged between the check node c_i and the variable node v_t for $\hat{P} = \hat{a}$, we denote the equivalent messages for $(\hat{H}_{it} \times \overline{\hat{P}}_t)$ as $\check{m}^{\hat{a}_s}_{c_i \to v_t}$ and $\check{m}^{\hat{a}_s}_{v_t \to c_i}$, respectively, where we have $(\hat{H}_{it} \times \overline{\hat{a}}) = \hat{a}_s$. Based on this notation, we may infer from Eq. (31) and Eq. (32) that the Probability Density Function (PDF) of the horizontal message $\check{m}^{\hat{a}_s}_{c_i \to v_t}$ can be obtained by convolving the PDFs of the messages $\check{m}^{\hat{a}_s + \hat{S}_i}_{v_{t'} \to c_i}$ for $v_{t'} \in V(c_i)\setminus v_t$. We may further notice in Eq. (31) that for a given S_i, $\hat{S}_i$ can have two possible values. More explicitly, for GF(4), we have $\mathrm{Tr}(0) = \mathrm{Tr}(1) = 0$, while $\mathrm{Tr}(\omega) = \mathrm{Tr}(\overline{\omega}) = 1$. Consequently, for $S_i = \mathrm{Tr}(\hat{S}_i = 0) = \mathrm{Tr}(\hat{S}_i = 1) = 0$, we have:

$$\begin{aligned} &PDF\{\check{m}^0_{c_i \to v_t}\} \\ &\quad = PDF\{\check{m}^1_{c_i \to v_t}\} \\ &\quad = \frac{1}{2}\left(\bigotimes_{v_{t'}} PDF\{\check{m}^0_{v_{t'} \to c_i}\} + \bigotimes_{v_{t'}} PDF\{\check{m}^1_{v_{t'} \to c_i}\}\right), \\ &PDF\{\check{m}^\omega_{c_i \to v_t}\} \\ &\quad = PDF\{\check{m}^{\overline{\omega}}_{c_i \to v_t}\} \\ &\quad = \frac{1}{2}\left(\bigotimes_{v_{t'}} PDF\{\check{m}^\omega_{v_{t'} \to c_i}\} + \bigotimes_{v_{t'}} PDF\{\check{m}^{\overline{\omega}}_{v_{t'} \to c_i}\}\right), \end{aligned} \tag{33}$$

where $\bigotimes$ represents the convolution process and $v_{t'} \in V(c_i)\setminus v_t$. Similarly, for $S_i = \mathrm{Tr}(\hat{S}_i = \omega) = \mathrm{Tr}(\hat{S}_i = \overline{\omega}) = 1$, we have:

$$\begin{aligned} &PDF\{\check{m}^0_{c_i \to v_t}\} \\ &\quad = PDF\{\check{m}^1_{c_i \to v_t}\} \\ &\quad = \frac{1}{2}\left(\bigotimes_{v_{t'}} PDF\{\check{m}^\omega_{v_{t'} \to c_i}\} + \bigotimes_{v_{t'}} PDF\{\check{m}^{\overline{\omega}}_{v_{t'} \to c_i}\}\right), \\ &PDF\{\check{m}^\omega_{c_i \to v_t}\} \\ &\quad = PDF\{\check{m}^{\overline{\omega}}_{c_i \to v_t}\} \\ &\quad = \frac{1}{2}\left(\bigotimes_{v_{t'}} PDF\{\check{m}^0_{v_{t'} \to c_i}\} + \bigotimes_{v_{t'}} PDF\{\check{m}^1_{v_{t'} \to c_i}\}\right). \end{aligned} \tag{34}$$

The complex convolution operation required in Eq. (33) and (34) can be efficiently implemented by multiplying the corresponding PDFs in the frequency domain with the aid of the FFT-based algorithm of [80].

C. DECODING ISSUES & HEURISTIC METHODS FOR IMPROVEMENT

Belief propagation invoked for decoding LDPC codes gives the exact solution only when the underlying Tanner graph is a tree. Nonetheless, it yields reasonably good approximations even in the presence of cycles, provided that the girth of the associated LDPC matrix is sufficiently large, at least 6. This has been proven by the capacity approaching classical LDPC codes, for example in [16] and [17]. Unfortunately, short cycles of length 4 are unavoidable in the construction of QLDPC codes, which in turn impair the iterative decoding procedure.

The unavoidable cycles of length 4 found in QLDPC codes are the result of the commutativity property of the stabilizers. More explicitly, the constituent stabilizer generators of a stabilizer code must commute, i.e. they should have even number of places with different non-Identity Pauli operators. In other words, if an anti-commuting pair of Pauli operators acts on the tth variable node in a pair of stabilizer generators, then there should be another anti-commuting pair of Pauli operators acting on the t'th variable node in the same pair of generators for the sake of ensuring that the generators commute with each other. For example, the generators:

$$\begin{aligned} g_0 &= \mathbf{XIYZ}, \\ g_1 &= \mathbf{ZYXI}, \end{aligned} \tag{35}$$

commute[18] because there are two pairs of anti-commuting Pauli operators acting on the first and third qubits, respectively. This in turn implies that the corresponding rows in the resultant PCM have even number of overlaps, which give rise to short cycles in the Tanner graph, as illustrated in Fig. 11. Since here the key point is to have ''different non-Identity operators'', a possible option could be to assign only a single type of non-Identity operator to each variable node of the Tanner graph. If we only assign Pauli-$\mathbf{X}$ to the variable node v_t so that it does not anti-commute in any pair of generators, then we will be unable to detect both Pauli-$\mathbf{X}$ as well as Pauli-$\mathbf{Y}$ errors acting on v_t. This would yield an undesirable code, which has a minimum distance of one. We may conclude that:

1) each column of a QLDPC matrix must have at least two different non-Identity Pauli operators, and
2) every pair of rows must an have even number of places with different non-Identity Pauli operators.

Consequently, all CSS as well as non-CSS QLDPC constructions have a Tanner graph of girth-4. It is interesting to observe here that these short cycles may be avoided in the corresponding binary formalism. Let us consider the example given in Eq. (35), which can be expressed in the binary form as follows:

$$\begin{aligned} g_0 &\rightarrow \begin{pmatrix} 1 & 0 & 1 & 0 & | & 0 & 0 & 1 & 1 \end{pmatrix}, \\ g_1 &\rightarrow \begin{pmatrix} 0 & 1 & 1 & 0 & | & 1 & 1 & 0 & 0 \end{pmatrix}. \end{aligned} \tag{36}$$

Since these binary[18] generators only have a single overlapping 1, the length 4 cycle no longer exits. However, let us recall from Section IV-B that binary decoding ignores the correlation between the $\mathbf{X}$ and $\mathbf{Z}$ errors, which degrades the performance. Hence, a compromise must be struck between these two conflicting aspects.

[18] This is just a random example to illustrate the concept of commutativity and the resulting short cycles. The generators g_0 and g_1 of this example may not constitute a good stabilizer code.

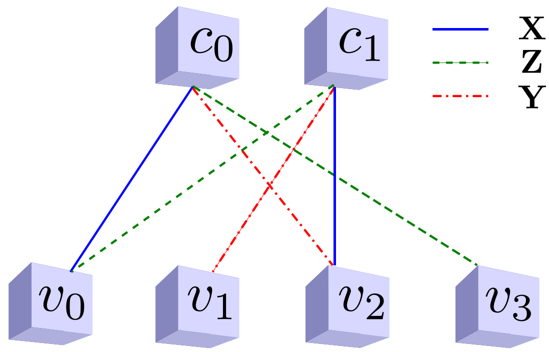

FIGURE 11. Tanner graph of a commuting pair of stabilizer generators, where c_0 and c_1 are the check nodes for the generators g_0 = XIYZ and g_1 = ZYXI, respectively. The edges connected to the variable nodes v_0 and v_2 constitute a cycle of length 4.

The issue of short cycles is more pronounced in both the dual-containing QLDPC codes as well as in the EA CSS QLDPC codes having $H'_x = H'_z$. We may call them homogeneous CSS codes, since identical PCMs are used for correcting bit-flips and phase-flips. Let the resultant $m \times n$ PCM in GF(4) be $\hat{H}$ as follows:

$$\hat{H} = \begin{pmatrix} \omega H'_z \\ H'_z \end{pmatrix}. \tag{37}$$

Consequently, the ith and $(i + m/2)$th rows completely overlap, resulting in numerous cycles of length 4. Furthermore, the dual-containing code construction also has the additional short cycles within the matrix H'_z, as discussed in Section III-A, which exist even in the binary formalism. Table 4 summarizes the presence of unavoidable short cycles in various code structures, while Fig. 12 captures the merits and demerits of GF(4) decoding as compared to its binary counterpart.

TABLE 4. Unavoidable short cycles in various code structures (✓ = present, ✗ = absent, ✔ = numerous cycles present).

Code Type	Unavoidable Short Cycles	
	Binary Formalism	GF(4) Formalism
Dual-containing CSS (Homogeneous)	✓	✔
Non-dual-containing CSS	✗	✓
Non-CSS	✗	✓
Homogeneous CSS EA	✗	✔
All other EA	✗	✗

Degeneracy is another unique aspect, which distinguishes a quantum code from a classical one. Let us recall from Section II that errors, which differ only by the stabilizer group, have the same impact on the transmitted codewords and can therefore be corrected by the same recovery operation. This in turn improves the performance of quantum codes. Unfortunately, the iterative decoding invoked for QLDPC codes does not take into account this degeneracy.

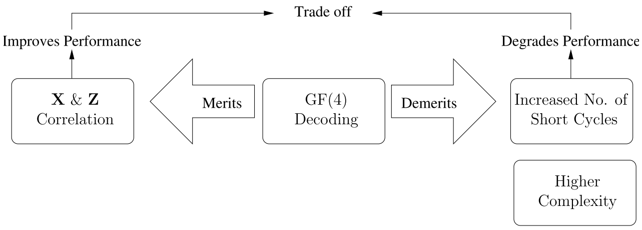

FIGURE 12. Merits and demerits of GF(4) decoding as compared to binary decoding.

More explicitly, rather than finding the most likely error, as in Eq. (23), the decoding algorithm should find the most likely error coset by summing the probabilities of all degenerate errors [81], [82]. Furthermore, QLDPC codes are highly degenerate as compared to the other families of quantum codes. This is because the generators of a QLDPC code are sparse in nature. Consequently, it has many low-weight degenerate errors, which dominate the probability of the error coset. It is therefore more likely that the most probable error $\tilde{P}$ of Eq. (23) may not coincide with the most probable error coset for QLDPC codes. However, rather than exploiting the benefits of high degeneracy associated with sparse codes, the marginalized iterative decoding invoked for QLDPC codes is impaired by degeneracy [81], [82]. This is because degenerate errors of equal weight have the same marginalized probability distribution, which can be attributed to the symmetry of the probability distribution of the channel depicted in Eq. (29).

Let us review the case study given in [81]. Consider a 2-qubit stabilizer code having the generators **XX** and **ZZ**. Assume furthermore that **IX** is the channel error encountered during transmission over a depolarizing channel, whose PDF is given in Eq. (29). The resultant syndrome is $S = (0\,1)$ and the corresponding set of degenerate errors is {**XI**, **IX**, **YZ**, **ZY**}. Consequently, the marginalized conditional probability of the error on each of the two qubits is given by:

$$\mathrm{P}\left(\hat{P}_t = \hat{a}|S\right) = \begin{cases} 1-p, & \text{if } \hat{a} = 0 \\ p/3, & \text{if } \hat{a} \in \{1, \omega, \overline{\omega}\}, \end{cases} \tag{38}$$

where $t = \{0, 1\}$. Hence, the marginalized probability is identical for both the qubits. This symmetry forces the decoder to detect the same error on both the qubits. However, none of the associated errors, i.e. {**XI**, **IX**, **YZ**, **ZY**}, exhibit this symmetry, hence leading to the 'symmetric degeneracy error' concept of [81]. Moreover, since the channel profile of Eq. (29) is biased towards the Identity operator, the probability of 'no-error' dominates at low noise levels.

Poulin and Chung investigated various heuristic methods in [81] to break the symmetry exhibited by the marginalized probabilities of Eq. (38). Among the investigated methods, "random perturbation" provides the best performance. It aims for breaking the degenerate symmetry by randomly perturbing the channel PDF of Eq. (29) for the qubits involved in the frustrated checks,[19] thus putting an end to the decoding impasse. Random perturbation begins with the standard non-binary BP, which gives the estimated channel error $\tilde{\hat{P}}$. If the syndrome computed for $\tilde{\hat{P}}$ is not the same as the observed channel syndrome S, the channel probabilities of all variable nodes v_t connected to a randomly chosen frustrated check c_i are perturbed (up to a normalization) as follows:

$$\begin{aligned} \mathbf{P}_{\mathrm{ch}}(\hat{P}_t = 0) &\rightarrow \mathbf{P}_{\mathrm{ch}}(\hat{P}_t = 0), \\ \mathbf{P}_{\mathrm{ch}}(\hat{P}_t = 1) &\rightarrow (1+\delta_1)\mathbf{P}_{\mathrm{ch}}(\hat{P}_t = 1), \\ \mathbf{P}_{\mathrm{ch}}(\hat{P}_t = \omega) &\rightarrow (1+\delta_\omega)\mathbf{P}_{\mathrm{ch}}(\hat{P}_t = \omega), \\ \mathbf{P}_{\mathrm{ch}}(\hat{P}_t = \overline{\omega}) &\rightarrow (1+\delta_{\overline{\omega}})\mathbf{P}_{\mathrm{ch}}(\hat{P}_t = \overline{\omega}), \end{aligned} \tag{39}$$

where δ_1, δ_ω and $\delta_{\overline{\omega}}$ are random variables in the range $[0, \delta]$. Non-binary BP is re-run with these modified channel probabilities for T_{pert} iterations and $\tilde{\hat{P}}$ is estimated again. If all the check nodes are satisfied now, the process terminates. Otherwise, the channel probabilities perturbed in Eq. (39) are restored and the process is repeated with another randomly chosen frustrated check.

Another heuristic method of alleviating the symmetric degeneracy problem was conceived in [83], which exploits an enhanced feedback procedure. More specifically, Wang *et al.* [83] proposed an "enhanced feedback" strategy for perturbing the channel probabilities similar to the random perturbation, but this perturbation is based both on the stabilizer generators involved in the frustrated checks as well as on the channel model. Similar to the random perturbation method, the enhanced feedback algorithm randomly selects a frustrated check c_i. It also selects a variable node v_t connected to c_i. Let $\tilde{S}_i$ be the value of the ith check node for the estimated error $\tilde{\hat{P}}$, while S_i be the ith observed channel syndrome. The channel probability for v_t is then perturbed as follows:

- If $\tilde{S}_i = 0$ and $S_i = 1$, then:

$$\mathbf{P}_{\mathrm{ch}}\left(\hat{P}_t = \hat{a}\right) = \begin{cases} p/2, & \text{if } \hat{a} = 0 \text{ or } \hat{H}_{it}, \\ (1-p)/2, & \text{otherwise.} \end{cases} \tag{40}$$

- If $\tilde{S}_i = 1$ and $S_i = 0$, then:

$$\mathbf{P}_{\mathrm{ch}}\left(\hat{P}_t = \hat{a}\right) = \begin{cases} (1-p)/2, & \text{if } \hat{a} = 0 \text{ or } \hat{H}_{it}, \\ p/2, & \text{otherwise.} \end{cases} \tag{41}$$

The perturbed values are fed to the standard non-binary BP decoder, which provides a new estimate of the channel error. The perturbation process is repeated, until all the checks are satisfied or the maximum number of feedbacks n_a is reached. Since these perturbations are more reliable than random perturbations, this method outperforms the random perturbation based heuristic method of [29].

V. MODIFIED NON-BINARY DECODING FOR HOMOGENEOUS CSS-TYPE QLDPC CODES

Let us recall from Section IV-C that homogeneous CSS-type QLDPC codes, which include both the dual-containing

[19] Check nodes for which the computed syndrome does not match the observed syndrome are known as frustrated checks [81].

construction as well as the EA-QLDPC codes, have an excessive number of short cycles. The ith and $(i+m/2)$th rows of the associated PCM $\hat{H}$ are related by a multiple of ω, i.e. we have $\hat{H}_i = \omega \hat{H}_{i+m/2}$, as seen in Eq. (37). For example, consider the 7-qubit Steane code [32], which is derived from the (7, 4) Hamming code. The PCM of a classical (7, 4) Hamming code is given by:

$$H'_z = \begin{pmatrix} 1 & 0 & 0 & 1 & 0 & 1 & 1 \\ 0 & 1 & 0 & 1 & 1 & 0 & 1 \\ 0 & 0 & 1 & 0 & 1 & 1 & 1 \end{pmatrix}. \tag{42}$$

Consequently, according to Eq. (37), the corresponding PCM of the 7-qubit Steane code is:

$$\hat{H} = \begin{pmatrix} \omega & 0 & 0 & \omega & 0 & \omega & \omega \\ 0 & \omega & 0 & \omega & \omega & 0 & \omega \\ 0 & 0 & \omega & 0 & \omega & \omega & \omega \\ 1 & 0 & 0 & 1 & 0 & 1 & 1 \\ 0 & 1 & 0 & 1 & 1 & 0 & 1 \\ 0 & 0 & 1 & 0 & 1 & 1 & 1 \end{pmatrix}, \tag{43}$$

whose Tanner graph is plotted in Fig. 13. As gleaned from Fig. 13, cycles of length 4 exist between all the variable nodes connected to the checks c_i and c_{i+3}. The dual-containing nature of Steane code also results in some additional short cycles. However, here we focus our attention only on the cycles resulting from the homogeneous CSS structure. To alleviate the impact of these short cycles, we propose a modified Tanner graph, which amalgamates the check nodes c_i and $c_{i+m/2}$ into a supernode, thereby eliminating the cycles. The resultant modified Tanner graph is given in Fig. 14. Based on the modified Tanner graph of Fig. 14, the horizontal messages exchanged between the supernodes $(c_i, c_{i+m/2})$ and the variable nodes v_t aim for satisfying both the checks c_i and $c_{i+m/2}$ simultaneously. Therefore, we have to modify Eq. (33) and (34) of the non-binary BP accordingly.

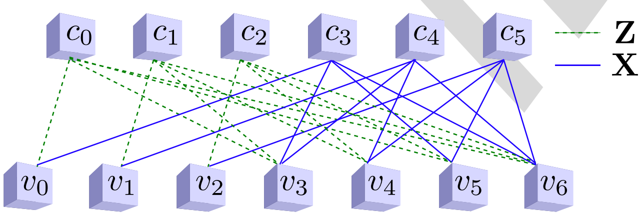

FIGURE 13. Tanner graph of the 7-qubit Steane code.

Since we have $\hat{H}_i = \omega \hat{H}_{i+m/2}$, $\hat{S}_i$ and $\hat{S}_{i+m/2}$ are also related similarly, i.e. we have $\hat{S}_i = \omega \hat{S}_{i+m/2}$. Based on this relation, Table 5 enlists the possible values of $\hat{S}_{i+m/2}$ for all the possible values of $\hat{S}_i$ along with the corresponding binary syndromes $S_i = \mathrm{Tr}(\hat{S}_i)$ and $S_{i+m/2} = \mathrm{Tr}(\hat{S}_{i+m/2})$. As gleaned from Table 5, for each value of S_i (or $S_{i+m/2}$), there are two possible values of $\hat{S}_i$ (or $\hat{S}_{i+m/2}$). Recall from Section IV-B that this is because $\mathrm{Tr}(0) = \mathrm{Tr}(1) = 0$, while $\mathrm{Tr}(\omega) = \mathrm{Tr}(\overline{\omega}) = 1$. On the other hand, for every pair of $(S_i, S_{i+m/2})$, there is a unique value of $\hat{S}_i$ and $\hat{S}_{i+m/2}$.

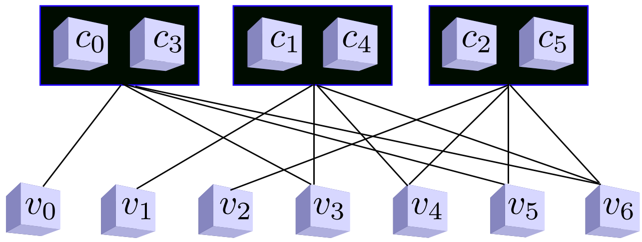

FIGURE 14. Modified Tanner graph of 7-qubit Steane code. Check nodes c_i and $c_{i+m/2}$ are combined to form a supernode.

TABLE 5. List of all possible values of $\hat{S}_i$ and the corresponding values of $\hat{S}_{i+m/2}$ and the binary syndromes $S_i = \mathrm{Tr}(\hat{S}_i)$ and $S_{i+m/2} = \mathrm{Tr}(\hat{S}_{i+m/2})$.

$\hat{S}_i$	$\hat{S}_{i+m/2}$	S_i	$S_{i+m/2}$
0	0	0	0
1	$\overline{\omega}$	0	1
ω	1	1	0
$\overline{\omega}$	ω	1	1

Consequently, for the supernode $C_i = (c_i, c_{i+m/2})$, the PDFs of Eq. (33) and (34) may be modified as follows:

- If the observed channel syndromes are $(S_i, S_{i+m/2}) = (0, 0)$, then:

$$PDF\{\check{m}^{\hat{a}_s}_{C_i \to v_t}\} = \bigotimes_{v_{t'}} PDF\{\check{m}^{\hat{a}_s}_{v_{t'} \to C_i}\}. \tag{44}$$

- If the observed channel syndromes obey $(S_i, S_{i+m/2}) = (0, 1)$, then we have:

$$PDF\{\check{m}^{\hat{a}_s}_{C_i \to v_t}\} = \bigotimes_{v_{t'}} PDF\{\check{m}^{\hat{a}_s+1}_{v_{t'} \to C_i}\}. \tag{45}$$

- If the observed channel syndromes satisfy $(S_i, S_{i+m/2}) = (1, 0)$, then we arrive at:

$$PDF\{\check{m}^{\hat{a}_s}_{C_i \to v_t}\} = \bigotimes_{v_{t'}} PDF\{\check{m}^{\hat{a}_s+\omega}_{v_{t'} \to C_i}\}. \tag{46}$$

- If the observed channel syndromes are $(S_i, S_{i+m/2}) = (1, 1)$, then:

$$PDF\{\check{m}^{\hat{a}_s}_{C_i \to v_t}\} = \bigotimes_{v_{t'}} PDF\{\check{m}^{\hat{a}_s+\overline{\omega}}_{v_{t'} \to C_i}\}. \tag{47}$$

Here $\hat{a}_s = (\hat{H}_{it} \times \overline{\hat{a}})$ for $\hat{a} \in \{0, 1, \omega, \overline{\omega}\}$.

Hence, Eq. (44) to (47) ensure that both the constituent check nodes c_i and $c_{i+m/2}$ of the supernode C_i are satisfied simultaneously. This is achieved without any additional complexity overhead. In fact, our proposed method requires less computations than the standard non-binary BP, because the number of check nodes is reduced to half.

Let us consider the Steane code of Eq. (43) for explaining the decoding procedure. Assume that when the 7-qubit codeword is transmitted over a quantum depolarizing channel having a depolarizing probability of $p = 0.26$, an **X** error is inflicted on the first qubit, i.e.

we have $\mathcal{P} = \mathbf{XIIIIII}$. Using Eq. (30), the observed syndrome may be computed as:

$$S = \mathrm{Tr}\left(\begin{pmatrix} \omega & 0 & 0 & \omega & 0 & \omega & \omega \\ 0 & \omega & 0 & \omega & \omega & 0 & \omega \\ 0 & 0 & \omega & 0 & \omega & \omega & \omega \\ 1 & 0 & 0 & 1 & 0 & 1 & 1 \\ 0 & 1 & 0 & 1 & 1 & 0 & 1 \\ 0 & 0 & 1 & 0 & 1 & 1 & 1 \end{pmatrix} \cdot \begin{pmatrix} 1 \\ 0 \\ 0 \\ 0 \\ 0 \\ 0 \\ 0 \end{pmatrix}\right)$$

$$= \mathrm{Tr}\begin{pmatrix} \omega \\ 0 \\ 0 \\ 1 \\ 0 \\ 0 \end{pmatrix} = \begin{pmatrix} 1 \\ 0 \\ 0 \\ 0 \\ 0 \\ 0 \end{pmatrix}. \tag{48}$$

We first run the standard non-binary BP on the Tanner graph of Fig. 13 for estimating the channel error. The non-binary BP algorithm proceeds as follows:

- **Initialization:** The messages $m^{\hat{a}}_{v_t \to c_i}$, which are sent from the variable nodes $v_t \in \{v_0, v_1, \ldots, v_6\}$ to the check nodes $c_i \in \{c_0, c_1, \ldots, c_5\}$ for $\hat{a} \in \{0, 1, \omega, \overline{\omega}\}$, are initialized according to the channel depolarizing probability of $p = 0.26$, i.e. we have:

$$m^{\hat{a}}_{v_t \to c_i} = \begin{cases} 0.74, & \text{if } \hat{a} = 0 \\ 0.0867, & \text{if } \hat{a} \in \{1, \omega, \overline{\omega}\}. \end{cases} \tag{49}$$

- **Horizontal message exchange:** The horizontal messages $m^{\hat{a}}_{c_i \to v_t}$ equivalent to Eq. (26), which are sent from the check nodes c_i to the variable nodes v_t, may be computed using the FFT-based algorithm of [80]. The algorithm is briefly outlined below:

  Step 1 (PDF of $\check{m}^{\hat{a}_s}_{v_t \to c_i}$): Recall from Section IV-B that we have:

$$\hat{a}_s = \hat{H}_{it} \times \overline{\hat{a}}. \tag{50}$$

  Consequently, the PDF of $\check{m}^{\hat{a}_s}_{v_t \to c_i}$ can be obtained by permuting the corresponding PDF of $m^{\hat{a}}_{v_t \to c_i}$ according to the value of $\hat{H}_{it}$ using Eq. (50). Let us consider the PDF of the message $m^{\hat{a}}_{v_0 \to c_0}$, which is equivalent to $(m^0_{v_0 \to c_0}, m^1_{v_0 \to c_0}, m^{\omega}_{v_0 \to c_0}, m^{\overline{\omega}}_{v_0 \to c_0})$. The corresponding entry in $\hat{H}$ is $\hat{H}_{00} = \omega$. Hence, using Eq. (50) and Table 2, we get $\hat{a}_s = (0, \omega, 1, \overline{\omega})$ for $\hat{a} = (0, 1, \omega, \overline{\omega})$. This implies that the PDF of $\check{m}^{\hat{a}_s}_{v_0 \to c_0}$ is equivalent to $(m^0_{v_0 \to c_0}, m^{\omega}_{v_0 \to c_0}, m^1_{v_0 \to c_0}, m^{\overline{\omega}}_{v_0 \to c_0})$. For the $\hat{H}$ of Eq. (43), we may generalize the computation of $\check{m}^{\hat{a}_s}_{v_t \to c_i}$ as follows:

$$PDF\{\check{m}^{\hat{a}_s}_{v_t \to c_i}\} = (m^0_{v_t \to c_i}, m^{\omega}_{v_t \to c_i}, m^1_{v_t \to c_i}, m^{\overline{\omega}}_{v_t \to c_i}), \tag{51}$$

  if $c_i \in \{c_0, c_1, c_2\}$, while we have:

$$PDF\{\check{m}^{\hat{a}_s}_{v_t \to c_i}\} = (m^0_{v_t \to c_i}, m^1_{v_t \to c_i}, m^{\omega}_{v_t \to c_i}, m^{\overline{\omega}}_{v_t \to c_i}), \tag{52}$$

  if $c_i \in \{c_3, c_4, c_5\}$. Furthermore, given the initial PDF of Eq. (49), Eq. (51) and Eq. (52) reduces to:

$$\check{m}^{\hat{a}_s}_{v_t \to c_i} = \begin{cases} 0.74, & \text{if } \hat{a}_s = 0 \\ 0.0867, & \text{if } \hat{a}_s \in \{1, \omega, \overline{\omega}\}, \end{cases} \tag{53}$$

  for $c_i \in \{c_0, c_1, \ldots, c_5\}$.

  Step 2 (FFT of the PDF of $\check{m}^{\hat{a}_s}_{v_t \to c_i}$): Recall from Section IV-B that the convolution operation required in Eq. (33) and Eq. (34) is equivalent to the multiplication of the corresponding PDFs in the frequency domain. The FFT of the PDF of Eq. (53) can be computed using the FFT matrix as follows:

$$\mathcal{F}\{\check{m}^{\hat{a}_s}_{v_t \to c_i}\} = \begin{pmatrix} 1 & 1 & 1 & 1 \\ 1 & -1 & 1 & -1 \\ 1 & 1 & -1 & -1 \\ 1 & -1 & -1 & 1 \end{pmatrix} \cdot \begin{pmatrix} \check{m}^0_{v_t \to c_i} \\ \check{m}^1_{v_t \to c_i} \\ \check{m}^{\omega}_{v_t \to c_i} \\ \check{m}^{\overline{\omega}}_{v_t \to c_i} \end{pmatrix}, \tag{54}$$

  where $\mathcal{F}$ denotes the FFT operation. Hence, the FFT of the PDF of Eq. (53) is equivalent to:

$$\mathcal{F}\{\check{m}^{\hat{a}_s}_{v_t \to c_i}\} = \begin{pmatrix} 1 \\ 0.6533 \\ 0.6533 \\ 0.6533 \end{pmatrix}. \tag{55}$$

  Step 3 (Convolution of PDFs): The convolution operations of Eq. (33) and Eq. (34), which are invoked for computing the horizontal messages related to the variable node v_t, can be carried out using the FFT as follows:

$$\bigotimes_{v_{t'}} PDF\{\check{m}^{\hat{a}_s}_{v_{t'} \to c_i}\} \equiv \mathcal{F}^{-1}\left\{\prod_{v_{t'}} \mathcal{F}\{\check{m}^{\hat{a}_s}_{v_{t'} \to c_i}\}\right\}, \tag{56}$$

  where $\mathcal{F}^{-1}$ denotes the Inverse FFT (IFFT) operation and $v_{t'} \in V(c_i) \backslash v_t$. Given the $\hat{H}$ of Eq. (43) and the FFT of Eq. (55), we get:

$$\prod_{v_{t'}} \mathcal{F}\{\check{m}^{\hat{a}_s}_{v_{t'} \to c_i}\} \equiv \begin{pmatrix} 1 \\ 0.2788 \\ 0.2788 \\ 0.2788 \end{pmatrix}. \tag{57}$$

  Then, the inverse FFT of Eq. (57) is computed by multiplying it with the FFT matrix, which is the same as that in Eq. (54). More explicitly, we have:

$$\mathcal{F}^{-1}\left\{\prod_{v_{t'}} \mathcal{F}\{\check{m}^{\hat{a}_s}_{v_{t'} \to c_i}\}\right\}$$

$$= \begin{pmatrix} 1 & 1 & 1 & 1 \\ 1 & -1 & 1 & -1 \\ 1 & 1 & -1 & -1 \\ 1 & -1 & -1 & 1 \end{pmatrix} \cdot \begin{pmatrix} 1 \\ 0.2788 \\ 0.2788 \\ 0.2788 \end{pmatrix} = \begin{pmatrix} 1.8364 \\ 0.7212 \\ 0.7212 \\ 0.7212 \end{pmatrix}. \tag{58}$$

Finally, the PDF of Eq. (58) is normalized to yield the output of Eq. (56), i.e. we get:

$$\bigotimes_{v_{t'}} PDF\{\check{m}^{\hat{a}_s}_{v_{t'}\rightarrow c_i}\} \equiv \begin{pmatrix} 0.4591 \\ 0.1803 \\ 0.1803 \\ 0.1803 \end{pmatrix}. \quad (59)$$

Step 4 (PDF of $\check{m}^{\hat{a}_s}_{c_i\rightarrow v_t}$): The PDF of the messages $\check{m}^{\hat{a}_s}_{c_i\rightarrow v_t}$ may be computed using Eq. (33) or Eq. (34) depending on the value of the syndrome observed, which was computed in Eq. (48). Since the syndrome of Eq. (48) is 1 for the first check node c_0, we use Eq. (34) for computing the PDF of the messages emerging from the check node c_0. Therefore, we get:

$$\check{m}^{\hat{a}_s}_{c_0\rightarrow v_t} = \begin{pmatrix} 0.1803 \\ 0.1803 \\ 0.3197 \\ 0.3197 \end{pmatrix}. \quad (60)$$

Furthermore, the syndrome of Eq. (48) has a value of 0 for all other check nodes. Therefore, we use Eq. (33) for $c_i \neq c_0$, which yields the following PDF:

$$\check{m}^{\hat{a}_s}_{c_i\rightarrow v_t} = \begin{pmatrix} 0.3197 \\ 0.3197 \\ 0.1803 \\ 0.1803 \end{pmatrix}. \quad (61)$$

Step 5 (PDF of $m^{\hat{a}}_{c_i\rightarrow v_t}$): For the sake of retrieving the messages $m^{\hat{a}}_{c_i\rightarrow v_t}$ from the PDF of $\check{m}^{\hat{a}_s}_{c_i\rightarrow v_t}$, the resultant PDFs of Eq. (60) and Eq. (61) have to be permuted, as we did in Step 1. More specifically, the permutation operation, which is required for this step, is the reverse of the permutation operation carried out in Step 1. Let us consider the check nodes $c_i \in \{c_0, c_1, c_2\}$, for which the non-zero values of $\hat{H}_{it}$ are always equal to ω (or equivalently all the branches emerging from these check nodes in the Tanner graph of Fig. 13 are labeled with the Pauli-**Z** operator). Furthermore, recall from Step 1 that $\hat{a}_s = (0, \omega, 1, \overline{\omega})$ for $\hat{a} = (0, 1, \omega, \overline{\omega})$, when $\hat{H}_{it} = \omega$. This implies that the PDF of $m^{\hat{a}}_{c_i\rightarrow v_t}$ is equivalent to $(\check{m}^{0}_{c_i\rightarrow v_t}, \check{m}^{\omega}_{c_i\rightarrow v_t}, \check{m}^{1}_{c_i\rightarrow v_t}, \check{m}^{\overline{\omega}}_{c_i\rightarrow v_t})$, for $c_i \in \{c_0, c_1, c_2\}$. For all other check nodes, the PDF of $m^{\hat{a}}_{c_i\rightarrow v_t}$ is the same as that of $\check{m}^{\hat{a}_s}_{c_i\rightarrow v_t}$, because we have $\hat{H}_{it} = 1$. Therefore, the resultant PDFs are as follows:

$$m^{\hat{a}}_{c_i\rightarrow v_t} = \begin{pmatrix} 0.1803 \\ 0.3197 \\ 0.1803 \\ 0.3197 \end{pmatrix}, \quad (62)$$

for $c_i = c_0$, while we have:

$$m^{\hat{a}}_{c_i\rightarrow v_t} = \begin{pmatrix} 0.3197 \\ 0.1803 \\ 0.3197 \\ 0.1803 \end{pmatrix}, \quad (63)$$

TABLE 6. **Marginal probability $P(P_t = \hat{a}|S)$ after the first iteration, when the standard non-binary BP decoding algorithm is invoked over the Tanner graph of the 7-qubit Steane code for transmission through a depolarizing channel having $p = 0.26$, which inflicts an X error on the first qubit, i.e. we have $\mathcal{P} =$ XIIIIII.**

t	$\hat{a}=0$	$\hat{a}=1$	$\hat{a}=\omega$	$\hat{a}=\overline{\omega}$	$\tilde{P}_t$
0	0.7189	0.1493	0.0475	0.0842	0
1	0.8552	0.0565	0.0565	0.03185	0
2	0.8552	0.0565	0.0565	0.03185	0
3	0.8392	0.0983	0.0313	0.0313	0
4	0.9205	0.0343	0.0343	0.0109	0
5	0.8392	0.0983	0.0313	0.0313	0
6	0.9100	0.0601	0.0191	0.0108	0

for $c_i \in \{c_1, c_2\}$, and we have:

$$m^{\hat{a}}_{c_i\rightarrow v_t} = \begin{pmatrix} 0.3197 \\ 0.3197 \\ 0.1803 \\ 0.1803 \end{pmatrix}, \quad (64)$$

for the remaining check nodes $c_i \in \{c_3, c_4, c_5\}$.

- **Vertical message exchange:** We next compute the vertical messages $m^{\hat{a}}_{v_t\rightarrow c_i}$ using Eq. (27). For example, consider the message $m^{\hat{a}}_{v_0\rightarrow c_0}$, which is destined from the variable node v_0 to the check node c_0. Since the variable node v_0 is only connected to c_0 and c_3 in the Tanner graph of Fig. 13, the message $m^{\hat{a}}_{v_0\rightarrow c_0}$ may be computed as:

$$m^{\hat{a}}_{v_0\rightarrow c_0} = K\, \mathrm{P_{ch}}(P_0 = \hat{a}) \times m^{\hat{a}}_{c_3\rightarrow v_0} = \begin{pmatrix} 0.8005 \\ 0.0937 \\ 0.0529 \\ 0.0529 \end{pmatrix}. \quad (65)$$

- **Element-wise marginal probability:** The element-wise marginal probabilities of the error on the variable node v_t, given the observed syndrome S, may be computed using Eq. (28). Let us consider again the variable node v_0, which is connected to check nodes c_0 and c_3. Consequently, the resultant marginal distribution of the error P_t inflicted on the variable node v_t may be computed as:

$$\begin{aligned} \mathrm{P}(P_0 = \hat{a}|S) &= K\, \mathrm{P_{ch}}(P_0 = \hat{a}) \times m^{\hat{a}}_{c_0\rightarrow v_0} \times m^{\hat{a}}_{c_3\rightarrow v_0} \\ &= \begin{pmatrix} 0.7189 \\ 0.1493 \\ 0.0475 \\ 0.0842 \end{pmatrix}. \end{aligned} \quad (66)$$

The process is repeated for all the variable nodes and the resultant marginalized probabilities are tabulated in Table 6.

- **Hard decision & syndrome check:** Finally, a hard decision is made for the sake of finding the most likely error $\tilde{P}_t$, which maximizes the marginal probability computed in the previous step. The resultant values of $\tilde{P}_t$ are listed in the last column of Table 6. More specifically, the probability of 'no-error' dominates for all the variable nodes. The specific syndrome corresponding to the resultant

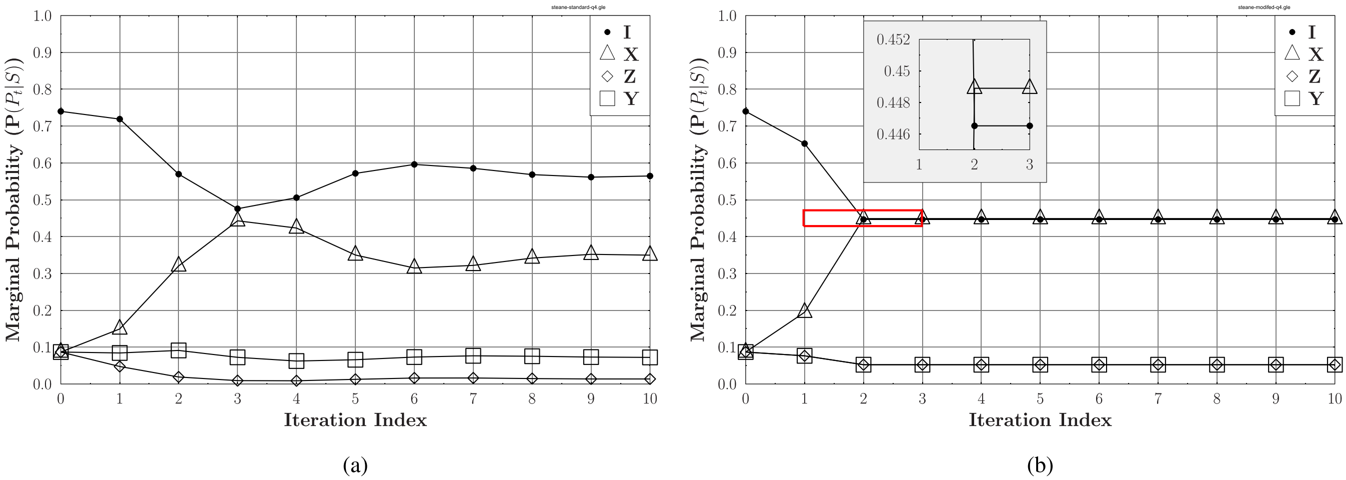

FIGURE 15. Evolution of the marginal probability for the first qubit of the 7-qubit Steane code for transmission through a depolarizing channel having $p = 0.26$, which inflicts an X error on the first qubit, i.e. we have $\mathcal{P} =$ XIIIIII. Standard BP fails to converge, while our modified BP converges to the correct solution in two iterations. (a) Standard non-binary BP. (b) Modified non-binary BP.

estimated error $\tilde{P}_t$ does not match the observed syndrome S of Eq. (48). Hence, the algorithm repeats itself from the horizontal message exchange step onwards.

Fig. 15a plots the resultant marginal probability $\mathrm{P}(P_t = \hat{a}|S)$ for the first qubit, as the iterations proceed. As seen from Fig. 15a, the standard decoding algorithm fails to converge. We next invoke our modified non-binary BP algorithm for the sake of analyzing the impact of the proposed algorithm. Recall from Fig. 14 that the check nodes c_i and c_{i+3} are amalgamated into a single supernode C_i. The corresponding observed syndrome values of Eq. (48) are also amalgamated, which yields $(S_0, S_3) = (1, 0)$, $(S_1, S_4) = (0, 0)$ and $(S_2, S_5) = (0, 0)$. Consequently, the modified BP differs from the standard non-binary BP in Step 4 of the 'horizontal message exchange', since it takes into account the amalgamated supernodes, rather than the individual check nodes. Using Eq. (44) to Eq. (47), Step 4 of the 'horizontal message exchange' may be carried out as follows:

- *Step 4 (PDF of $\check{m}^{\hat{a}_s}_{c_i \to v_t}$):* Since the syndrome observed for the supernode C_0 is $(S_0, S_3) = (1, 0)$, we use Eq. (46) for computing the PDF of the messages emerging from this supernode. Consequently, we arrive at:

$$\check{m}^{\hat{a}_s}_{C_0 \to v_t} = \bigotimes_{v_{t'}} PDF\{\check{m}^{\hat{a}_s+\omega}_{v_{t'} \to C_0}\} = \begin{pmatrix} 0.1803 \\ 0.1803 \\ 0.4591 \\ 0.1803 \end{pmatrix}. \quad (67)$$

Furthermore, since the syndrome is $(S_i, S_{i+3}) = (0, 0)$ for all other supernodes, we use Eq. (44) for computing the corresponding PDFs. Hence, we get:

$$\check{m}^{\hat{a}_s}_{C_i \to v_t} = \bigotimes_{v_{t'}} PDF\{\check{m}^{\hat{a}_s}_{v_{t'} \to C_i}\} = \begin{pmatrix} 0.4591 \\ 0.1803 \\ 0.1803 \\ 0.1803 \end{pmatrix}, \quad (68)$$

for $C_i \in \{C_1, C_2\}$.

The rest of the decoding algorithm is the same as the standard non-binary BP, except that we only have three supernodes in the modified Tanner graph of Fig. 14 in contrast to the six check nodes of Fig. 13. The resultant marginalized probabilities are tabulated in Table 7, while Fig. 15b plots the marginal probability for the first qubit, as the iterations proceed. We may observe in Fig. 15b that our modified BP algorithm converges to the correct estimate in as few as two iterations.

TABLE 7. Marginal probability $\mathrm{P}(P_t = \hat{a}|S)$ after the first iteration, when the modified non-binary BP decoding algorithm is invoked over the Tanner graph of the 7-qubit Steane code for transmission through a depolarizing channel having $p = 0.26$, which inflicts an X error on the first qubit, i.e. we have $\mathcal{P} =$ XIIIIII.

t	$\hat{a} = 0$	$\hat{a} = 1$	$\hat{a} = \omega$	$\hat{a} = \overline{\omega}$	$\tilde{P}_t$
0	0.1946	0.6525	0.0764	0.0764	0
1	0.8788	0.0404	0.0404	0.0404	0
2	0.8788	0.0404	0.0404	0.0404	0
3	0.8271	0.0969	0.0380	0.0380	0
4	0.9486	0.0171	0.0171	0.0171	0
5	0.8271	0.0969	0.0380	0.0380	0
6	0.9241	0.0425	0.0167	0.0167	0

VI. REWEIGHTED BP FOR GRAPHS EXHIBITING CYCLES

Belief propagation is capable of providing a reasonably good approximation to the optimization problem of Eq. (24), provided that the underlying Tanner graph has a sufficiently high girth. However, it is not guaranteed to converge or may converge onto an incorrect solution in the presence of cycles [84], [85]. Furthermore, it may require a large number of iterations for achieving convergence, especially in the high noise regime, thereby imposing a higher complexity. These shortcomings of the classic BP algorithm are primarily due to the fact that the BP messages become dependent with time when short cycles exist in the Tanner graph. Alternatively, we may refer to the messages as being 'over-confident' or 'over-estimated'. To alleviate the impact of this over-confidence, Wainwright *et al.* [84] conceived the Tree-Reweighted Belief Propagation (TRW-BP) method for pair-wise interactions, which improves the convergence of the classic BP by reweighting the edges of the underlying graph with their Edge Appearance Probabilities (EAP).[20] The TRW-BP algorithm was extended to higher-order interactions in [23] and [24], whereby EAPs were replaced by the Factor Appearance Probabilities (FAPs) of the nodes.[21] Based on this extended TRW-BP, Wymeersch *et al.* re-formulated the vertical message exchange step of the classic BP (Eq. (27)) as [23], [24]:

$$m^a_{v_t \to c_i} = K\, \mathrm{P_{ch}}(P_t = a) \left(m^a_{c_i \to v_t}\right)^{\rho_i - 1} \prod_{c_{i'} \in C(v_t) \backslash c_i} \left(m^a_{c_{i'} \to v_t}\right)^{\rho_{i'}}, \tag{69}$$

where ρ_i is the FAP of the ith check node. Similarly, the computation of the element-wise marginal probability (Eq. (28)) was modified as:

$$\mathrm{P}(P_t = a|S) = K \mathrm{P_{ch}}(P_t = a) \prod_{c_i \in C(v_t)} \left(m^a_{c_i \to v_t}\right)^{\rho_i}. \tag{70}$$

Both Eq. (69) and (70) reduces to the classic BP for $\rho_i = 1\ \forall i$.

The TRW-BP technique requires the optimization of ρ_i for all nodes. To reduce this optimzation task, Wymeersch *et al.* [23], [24] also proposed the URW-BP, which invokes a uniform FAP value for all the nodes, where we have $\rho_i = \rho\ \forall i$. Various other variations of TRW-BP have been investigated in [86]–[89] for classical binary LDPC codes, which demonstrate that the TRW-BP effectively improves the convergence of binary LDPC codes, when the number of iterations is not too high. Inspired by these results, in Section VII we also analyze the impact of URW-BP on the non-binary decoding of quantum LDPC codes, which are known to have unavoidable short cycles.

TABLE 8. System I - simulation parameters.

QLDPC Matrix	
Code Construction	Mackay's bicycle code
Coded qubits	$n = 800$
Information qubits	$k = 400$
E-bits	$c = 0$
Row weight	30
QLDPC Decoder	
Standard decoding iterations	$\mathtt{I}_{\max} = 90$
Perturbation iterations	$T_{\text{pert}}=40$
Random perturbation strength	$\delta = 0.1$
Maximum no. of feedbacks	$n_a = 40$

VII. RESULTS AND DISCUSSIONS

A. MODIFIED NON-BINARY DECODING

For the sake of quantifying the attainable performance gain of our modified non-binary BP of Section V, in this section we compare its performance in conjunction with the decoding algorithms of Section IV. Our first system of Table 8 relies on Mackay's 1/2-rate [800, 400] bicycle code having a row weight of 30. The corresponding WER performance recorded for various channel depolarizing probabilities is plotted in Fig. 16, where we have considered the following decoders:

1) **Binary:** the binary BP decoding algorithm of Section IV-A,
2) **Standard Non-Binary:** the non-binary BP decoding algorithm of Section IV-B,
3) **Random Perturbation:** the random perturbation technique [81] of Section IV-C,
4) **Enhanced Feedback:** the enhanced feedback method [83] of Section IV-C,
5) **Modified Non-Binary:** our modified non-binary BP of Section V,
6) **Modified & Enhanced Feedback:** our modified non-binary BP of Section V amalgamated with the enhanced feedback method [83] of Section IV-C.

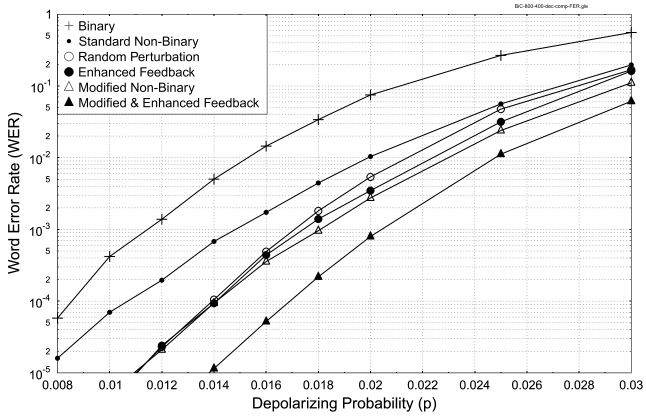

FIGURE 16. Achievable WER performance comparison of the modified BP with the existing decoding schemes, using the simulation parameters of Table 8.

For all the decoding schemes, we have used a maximum of $\mathtt{I}_{\max} = 90$ iterations. Furthermore, for both the 'Random Perturbation' as well as for the 'Enhanced Feedback', we set $T_{\text{pert}} = 40$, while the random perturbation strength was set to $\delta = 0.1$ and the maximum number of feedbacks to $n_a = 40$ for the 'Enhanced Feedback'.[22] These simulation parameters are tabulated in Table 8. Each decoding algorithm iterates until either a valid error is found or the maximum number of iterations is reached. Furthermore, the WER metric here counts both the detected as well as the undetected block errors.

We may observe in Fig. 16 that the 'Binary' decoder exhibits the worse performance. Using the 'Binary' decoder, we achieve a WER of 10^{-4} at a channel depolarizing probability of $p = 0.0085$, which increases to $p = 0.01075$ with the 'Standard Non-Binary' decoder. This is equivalent to a $\left(\frac{(0.01075-0.0085)}{0.0085} \times 100\right) = 26\%$ depolarizing probability increase that the decoder can cope with. Furthermore, the 'Random Perturbation', the 'Enhanced Feedback' and the

[20] EAP of an edge represents the probability of appearance of that edge in a randomly chosen spanning tree.

[21] FAP denotes the appearance probability of a node in the collection of trees [23], [24].

[22] We have used the decoding parameters of [83].

'Modified Non-Binary' decoders have a similar performance at low noise levels, increasing the tolerable depolarizing probability to $p = 0.014$ at a WER of 10^{-4}, which corresponds to a $(\frac{(0.014-0.01075)}{0.01075} \times 100) = 30\%$ increase of p at WER $= 10^{-4}$ with respect to the 'Standard Non-Binary' decoder. Furthermore, with the 'Modified & Enhanced Feedback' configuration, the tolerable depolarizing probability increases to $p = 0.017$ at a WER of 10^{-4}, which is equivalent to about $(\frac{(0.017-0.014)}{0.014} \times 100) = 21\%$ increase with respect to $p = 0.014$. Table 9 summarizes these results.

TABLE 9. Achievable depolarizing probability (p) at a WER of 10^{-4}, based on Fig. 16.

Dec. No.	Decoding Method	p	Improvement
1	Binary	0.0085	-
2	Standard Non-Binary	0.01075	26% w.r.t. Dec. 1
3	Random Perturbation	0.014	30% w.r.t. Dec. 2
4	Enhanced Feedback	0.014	30% w.r.t. Dec. 2
5	Modified Non-Binary	0.014	30% w.r.t. Dec. 2
6	Modified & Enhanced Feedback	0.017	21% w.r.t. Dec. 5

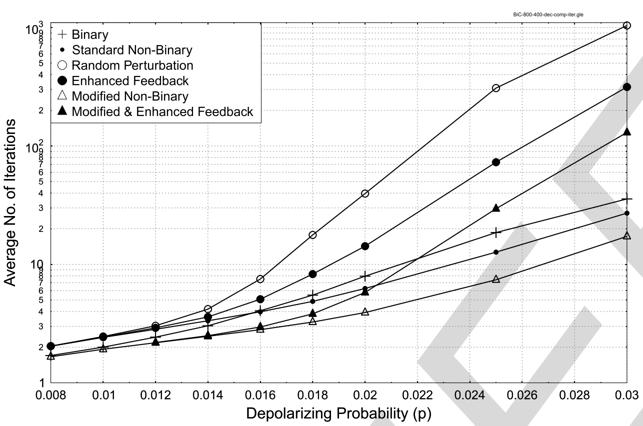

FIGURE 17. Comparison of the average number of decoding iterations invoked by the modified BP and the existing decoding schemes using the simulation parameters of Table 8.

The performance of our 'Modified Non-Binary' BP at a WER of 10^{-4} is similar to that of the heuristic methods, namely 'Random Perturbation' and 'Enhanced Feedback'. However, the 'Modified Non-Binary' technique imposes a lower decoding complexity in terms of the average number of decoding iterations, which is evidenced in Fig. 17. Consequently, our 'Modified Non-Binary' BP converges faster than the existing decoding schemes. In particular, in the high-noise regime, our 'Modified Non-Binary' decoder outperforms both the 'Random Perturbation' and the 'Enhanced Feedback' in terms of its WER performance recorded in Fig. 16 as well as in terms of the average number of iterations seen in Fig. 17. As compared to the 'Standard Non-Binary' decoder, the 'Modified Non-Binary' algorithm always yields a lower WER and invokes on average less decoding iterations. We may observe furthermore in Fig. 17 that the amalgamated 'Modified & Enhanced Feedback' invokes less iterations as compared to the 'Enhanced Feedback', while the performance of the former is also superior in terms of the WER curve of Fig. 16. This is again due to the fact that the modified BP of Section V facilitates faster convergence as compared to the standard non-binary decoding. More specifically, in the region of interest, i.e. for $p \leq 0.017$ corresponding to the desired WER of $\leq 10^{-4}$, the combination of the enhanced feedback method with our modified BP, namely 'Modified & Enhanced Feedback', imposes almost the same complexity as that imposed by the 'Modified Non-Binary' BP, when used on its own. However, the former exhibits a much lower WER than the latter. We compare furthermore the performance of all the decoding schemes at a depolarizing probability of $p = 0.016$ in Table 10.

TABLE 10. Performance comparison in terms of the achievable WER and the average number of decoding iterations (I_{avg}) invoked at a depolarizing probability of $p = 0.016$, based on Fig. 16 and Fig. 17.

Dec. No.	Decoding Method	WER	I_{avg}
1	Binary	1.5710^{-2}	3.98
2	Standard Non-Binary	1.4710^{-3}	4.28
3	Random Perturbation	4.5710^{-4}	7.52
4	Enhanced Feedback	4.4710^{-4}	5.08
5	Modified Non-Binary	3.6710^{-4}	2.81
6	Modified & Enhanced Feedback	5.2710^{-5}	2.96

TABLE 11. System II - Simulation parameters.

QLDPC Matrix	
Code Construction	Homogeneous EA-QLDPC
Coded qubits	$n = 816$
Information qubits	$k = 404$
E-bits	$c = 404$
Row weight	6
Column weight	3
QLDPC Decoder	
Standard decoding iterations	$\mathrm{I}_{max} = 90$
Perturbation iterations	$T_{pert} = 40$
Random perturbation strength	$\delta = 0.1$
Maximum no. of feedbacks	$n_a = 81$

Let us now compare the performance of the different decoding schemes in the context of our second system of Table 11, relying on the homogeneous EA-QLDPC code of [83] having $n = 816$, $k = 404$ and $e = 404$, which is derived from the Mackay's classical $(816, 408)$ LDPC, having a row weight of 6 and a column weight of 3. For all the decoding schemes, we have used a maximum of $\mathrm{I}_{max} = 90$ iterations. Furthermore, for both the 'Random Perturbation' as well as for the 'Enhanced Feedback' methods, we set $T_{pert} = 40$, while the random perturbation strength was set to $\delta = 0.1$ and the maximum number of feedbacks $n_a = 81$ was used for the 'Enhanced Feedback' decoder. These simulation parameters are summarized in Table 11. The resultant WER performance curves are compared in Fig. 18, while the average number of decoding iterations invoked for varying channel depolarizing probabilities are compared in Fig. 19. As observed from Fig. 18, the 'Binary' decoder achieves a WER of 10^{-4} at $p = 0.057$, which increases to $p = 0.069$ when the 'Standard Non-Binary' decoder is invoked. Consequently, the 'Standard Non-Binary' increases the tolerable depolarizing

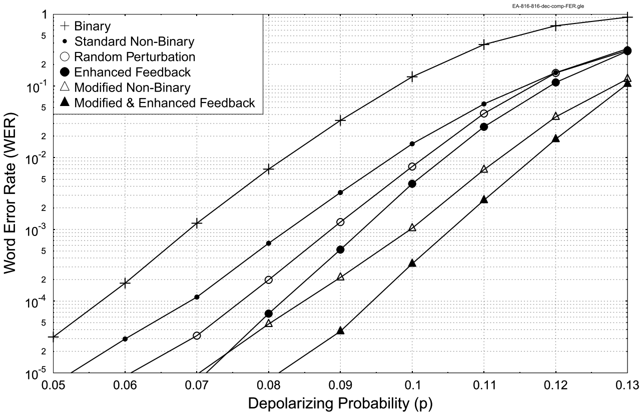

FIGURE 18. Achievable WER performance comparison of the modified BP with the existing decoding schemes, using the simulation parameters of Table 11.

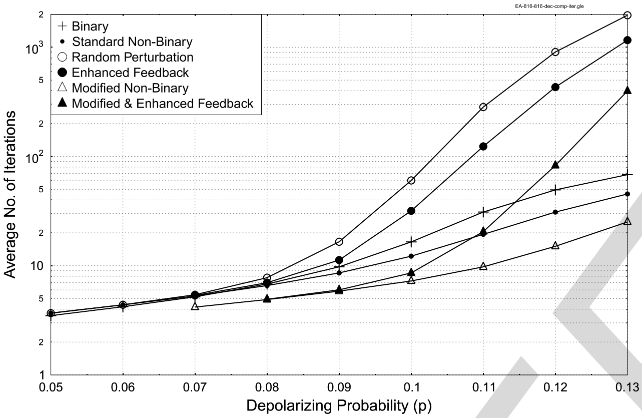

FIGURE 19. Comparison of the average number of decoding iterations invoked by the modified BP and the existing decoding schemes using the simulation parameters of Table 11.

probability by ($\frac{(0.069-0.057)}{0.057} \times 100) = 21\%$ as compared to the 'binary' decoder. This is further increased to $p = 0.076$ in conjunction with the 'Random Perturbation', which corresponds to about ($\frac{(0.076-0.069)}{0.069} \times 100) = 10\%$ increase and to $p = 0.082$ for the 'Enhanced Feedback', which represents a ($\frac{(0.082-0.069)}{0.069} \times 100) = 19\%$ increase. By contrast, our 'Modified Non-Binary' BP exhibits a WER of 10^{-4} around $p = 0.085$, which corresponds to a ($\frac{(0.085-0.069)}{0.069} \times 100) = 23\%$ increase as compared to the 'Standard Non-Binary' decoder. Using the heuristic enhanced feedback approach with our modified BP, namely 'Modified & Enhanced Feedback' provides a further increase to $p = 0.0945$, which represents a ($\frac{(0.0945-0.085)}{0.085} \times 100) = 11\%$ increase. These results are tabulated in Table 12. In terms of the average number of decoding iterations, our 'Modified Non-Binary' BP always outperforms both the 'Standard Non-Binary' decoder as well as the 'Random perturbation' and the 'Enhanced Feedback' solutions, as depicted in Fig. 19.

B. UNIFORMLY-REWEIGHTED BP

Since bicycle codes exhibit numerous short cycles, we use our first system of Table 8 for the analysis of the URW-BP

TABLE 12. Achievable depolarizing probability (p) at a WER of 10^{-4}, based on Fig. 18.

Dec. No.	Decoding Method	p	Improvement
1	Binary	0.057	-
2	Standard Non-Binary	0.069	21% w.r.t. Dec. 1
3	Random Perturbation	0.076	10% w.r.t. Dec. 2
4	Enhanced Feedback	0.082	19% w.r.t. Dec. 2
5	Modified Non-Binary	0.085	23% w.r.t. Dec. 2
6	Modified & Enhanced Feedback	0.0945	11% w.r.t. Dec. 5

of Section VI, which is combined with our modified non-binary decoder of Section V. More precisely, we amalgamate the horizontal exchange step of our modified non-binary BP with the vertical exchange step of the URW-BP.

We commence by heuristically determining the optimum value ρ of the FAP, which varies with both the channel depolarizing probability as well as with the maximum number of decoding iterations. Fig. 20 shows the impact of ρ on the WER performance at varying channel depolarizing probabilities p for $\mathtt{I}_{\max} = 10$, 20 and 90 iterations. We may observe in Fig. 20 that the WER varies with the value of ρ, attaining a minimum value at the optimum ρ. This optimum ρ is different for each p value, tending to move towards $\rho = 1$ as the value of p increases or as the maximum affordable number of iterations increases. The resultant values of ρ optimized for different channel depolarizing probabilities p and for different maximum number of iterations are summarized in Table 13.

TABLE 13. Optimized ρ for different values of p and maximum number of iterations $\mathtt{I}_{\max}$ for System I of Table 8, based on the performance curves of Fig. 20.

$\mathtt{I}_{\max}$	Optimized ρ for different values of p						
	0.012	**0.014**	**0.016**	**0.018**	**0.02**	**0.025**	**0.03**
10	0.8	0.8	0.8	0.9	0.9	0.9	0.9
20	0.8	0.8	0.9	0.9	0.9	0.9	1
90	0.9	0.9	0.9	0.9	0.9	1	1

To quantify the performance gain achieved with the aid of the URW-BP, we compare the performance of the optimized URW-BP to our modified non-binary BP in Fig. 21 for $\mathtt{I}_{\max} = 10$, 20 and 90 iteration. Here the optimized URW-BP is based on the best values of ρ listed in Table 13. The performance curves of Fig. 21 reveal that the improvement in WER is lower for higher values of p as well as for larger values of the maximum number of affordable iterations. For example, when a maximum of $\mathtt{I}_{\max} = 10$ decoding iterations are invoked at a WER of 10^{-3}, the URW-BP scheme increases $p = 0.0125$ to $p = 0.0155$, which is around a ($\frac{(0.0155-0.0125)}{0.0125} \times 100) = 24\%$ increase. By contrast, for a maximum of $\mathtt{I}_{\max} = 20$ iterations, URW-BP increases from $p = 0.015$ to $p = 0.017$ at a WER of 10^{-3}. This is equivalent to an increase of ($\frac{(0.017-0.015)}{0.015} \times 100) = 13\%$. Furthermore, at an even higher maximum number of iterations of $\mathtt{I}_{\max} = 90$, URW-BP achieves a WER of 10^{-3} at $p = 0.0185$, which is only a ($\frac{(0.0185-0.018)}{0.018} \times 100) = 3\%$ increase as compared to the modified non-binary algorithm.

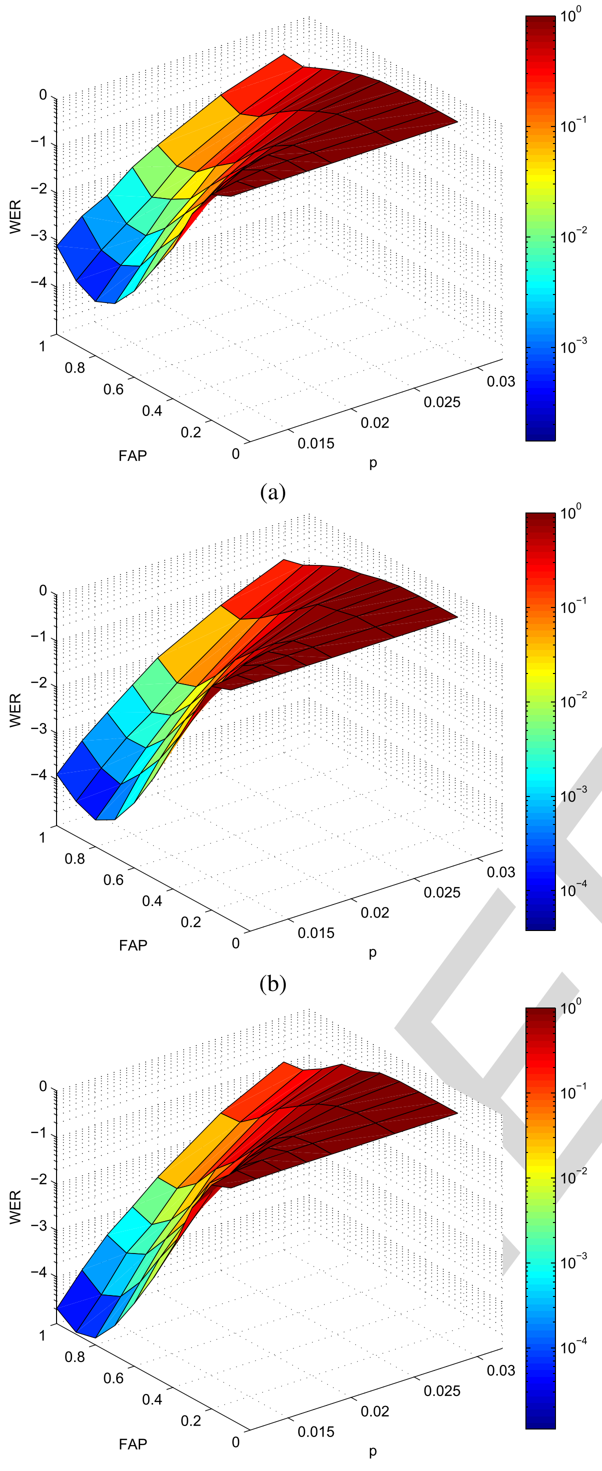

FIGURE 20. URW-BP optimization: impact of varying FAP values on the WER performance at various channel depolarizing probabilities *p*. URW-BP is amalgamated with the modified non-binary decoder and the performance is analyzed for the System I of Table 8. (a) $\mathtt{I}_{\mathbf{max}} = 10$ iterations. (b) $\mathtt{I}_{\mathbf{max}} = 20$ iterations. (c) $\mathtt{I}_{\mathbf{max}} = 90$ iterations.

These values are summarized in Table 14. Hence, the notion of reweighting the message probabilities is more beneficial at low depolarizing probabilities and for smaller values of the

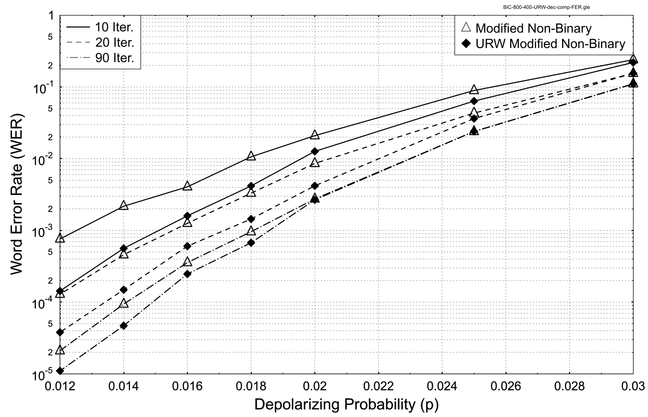

FIGURE 21. Achievable WER performance of the URW-BP, having the best values of ρ listed in Table 13, compared with the 'Modified Non-Binary', when used on its own. Performance is evaluated for the System I of Table 8 using $\mathtt{I}_{\mathbf{max}} = 10$, 20 and 90 iterations.

TABLE 14. Performance comparison of URW-BP with the modified BP for System I of Table 8, based on Fig. 21.

$\mathtt{I}_{\max}$	p at a WER of 10^{-3}		Increase
	Modified BP	**URW-BP**	
10	0.0125	0.0155	24%
20	0.015	0.017	13%
90	0.018	00185	3%

maximum affordable number of iterations. This is because at higher depolarizing probabilities (and similarly larger values of the maximum number of iterations), the messages are highly correlated.

VIII. CONCLUSIONS AND DESIGN GUIDELINES

QLDPC codes may be constructed from the classical binary as well as quaternary codes by imposing the stringent symplectic criterion on the resultant PCM, which ensures that the stabilizer generators commute with each other. The design guidelines of constructing QLDPC codes may be summarized as follows:

- An $[n, k]$ QLDPC code, having a coding rate of $R_Q = k/n$, may be constructed from a classical $(2n, n+k)$ binary LDPC code, having a coding rate of $R_c = (n+k)/2n$, if the associated PCM H satisfies the stringent symplectic criterion.
- Ideally, the rows of the PCM H should have at most a single overlapping value of 1 (or non-zero value in the GF(4) formalism)) for the sake of avoiding length-4 cycles in the Tanner graph, which degrade the performance of the iterative decoding algorithm. Unfortunately, the symplectic criterion requires 'even overlaps' between the rows of H, thus resulting in unavoidable length-4 cycles. A major design challenge is therefore to construct good QLDPC codes in the wake of the unavoidable length-4 cycles.
- We may exploit four main global structures of the PCM H for designing QLDPC codes, namely dual-containing CSS, non-dual-containing CSS, non-CSS

and the entanglement-assisted solutions of Fig. 4. The design challenges associated with each of these structures are summarized below:

- **Dual-containing CSS (Section III-A):** Mackay's bicycle codes are so far the best amongst the dual-containing CSS codes, but their performance is still not on par with the classical LDPC codes. This is because this construction suffers the most from having short cycles, which exist both in the binary as well as in the GF(4) formalism.
- **Non-dual-containing CSS codes (Section III-A):** It is difficult to find a pair of sparse binary PCMs satisfying the symplectic criterion, which constitute good QLDPC codes. At the time of writing, only the SC QC-LDPC codes and the non-binary QC-QLDPC codes are known to perform close to the Hashing bound. But this comes either at the cost of pre-shared noiseless ebits or at an increased complexity.
- **Non-CSS codes (Section III-B):** Ideally, non-CSS constructions are preferred over the CSS codes because they exploit the redundant qubits more efficiently. However, finding good non-CSS QLDPC codes remains an open challenge at the time of writing.
- **EA codes (Section III-C):** Entanglement-assistance may assist us in achieving a performance comparable to that of the classical LDPC codes. However again, this requires pre-shared ebits, which constitute a valuable resource gleaned at the cost of a transmission overhead. Therefore, efforts must be made to minimize the number of required ebits.

- Additionally, it is desirable that the resultant QLDPC code has the following attributes:
  - A structured PCM, for example a cyclic or quasi-cyclic structure, for facilitating its implementation; and
  - An unbounded minimum distance or at least a sufficiently high minimum distance for long block lengths.

QLDPC codes may be decoded using syndrome-based BP either in the binary domain or in the non-binary domain. Besides the obvious lower complexity of the binary decoding, the two main differences between these decoding regimes are:

- In contrast to the binary decoding, which assumes that the bit-flips and phase-flips are independent, non-binary decoding takes into account the correlation between them, which improves their performance.
- The number of length-4 cycles is higher in the non-binary formalism of the PCM as compared to the binary one. This tends to degrade the performance of the non-binary decoder.

Hence, we have a pair of conflicting attributes. However, the non-binary BP outperformed the binary BP for both QLDPC codes, which we investigated in this paper.

From the perspective of decoding, the challenges may be summarized as follows:

- **Degeneracy:** Quantum codes are inherently degenerate in nature. This may improve the associated decoding performance if the decoder takes this degeneracy into account. Unfortunately, the BP algorithm does not exploit this degeneracy. In fact, since BP is based on marginalized probabilities, the presence of degenerate errors impairs its performance.
- **Short cycles:** Unavoidable length-4 cycles found in QLDPC codes degrade the performance of BP. This gets even worse for the homogeneous CSS codes, when they are decoded in the non-binary domain.

Heuristic methods, namely random perturbation and enhanced feedback, are known to alleviate both these issues to some extent. However, this is achieved at the cost of an increased decoding complexity. Therefore, we conceive a modified non-binary decoding algorithm for homogeneous CSS-type QLDPC codes, which successfully alleviates the issue of unavoidable length-4 cycles. Our modified decoder exhibits a superior WER performance, despite its lower decoding complexity as compared to the state-of-the-art decoding techniques. It may also be amalgamated with heuristic methods for attaining additional performance gains. We also demonstrated that URW-BP can be exploited for counteracting the issues of short-cycles.

REFERENCES

[1] L. Hanzo, H. Haas, S. Imre, D. O'Brien, M. Rupp, and L. Gyongyosi, "Wireless myths, realities, and futures: From 3G/4G to optical and quantum wireless," *Proc. IEEE*, vol. 100, pp. 1853–1888, May 2012. AQ:3

[2] P. Botsinis, S. X. Ng, and L. Hanzo, "Quantum search algorithms, quantum wireless, and a low-complexity maximum likelihood iterative quantum multi-user detector design," *IEEE Access*, vol. 1, pp. 94–122, 2013. [Online]. Available: http://ieeexplore.ieee.org/xpl/articleDetails.jsp?arnumber=6515077 AQ:4

[3] D. Alanis, P. Botsinis, S. X. Ng, and L. Hanzo, "Quantum-assisted routing optimization for self-organizing networks," *IEEE Access*, vol. 2, pp. 614–632, 2014.

[4] D. Alanis, P. Botsinis, Z. Babar, S. X. Ng, and L. Hanzo, "Non-dominated quantum iterative routing optimization for wireless multihop networks," *IEEE Access*, vol. 3, pp. 1704–1728, 2015.

[5] P. Botsinis, D. Alanis, Z. Babar, S. X. Ng, and L. Hanzo, "Noncoherent quantum multiple symbol differential detection for wireless systems," *IEEE Access*, vol. 3, no. 99, pp. 569–598, 2015. AQ:5

[6] P. Botsinis, D. Alanis, Z. Babar, S. X. Ng, and L. Hanzo, "Iterative quantum-assisted multi-user detection for multi-carrier interleave division multiple access systems," *IEEE Trans. Commun.*, vol. 63, no. 10, pp. 3713–3727, Oct. 2015.

[7] S. Wiesner, "Conjugate coding," *SIGACT News*, vol. 15, no. 1, pp. 78–88, Jan. 1983. [Online]. Available: http://doi.acm.org/10.1145/1008908.1008920

[8] C. H. Bennett and G. Brassard, "Quantum cryptography: Public key distribution and coin tossing," in *Proc. IEEE Int. Conf. Comput., Syst., Signal Process.*, New York, NY, USA, Dec. 1984, pp. 175–179.

[9] A. Beige, B.-G. Englert, C. Kurtsiefer, and H. Weinfurter, "Secure communication with single-photon two-qubit states," *J. Phys. A, Math. General*, vol. 35, no. 28, p. L407, 2002. [Online]. Available: http://stacks.iop.org/0305-4470/35/i=28/a=103

[10] K. Boström and T. Felbinger, "Deterministic secure direct communication using entanglement," *Phys. Rev. Lett.*, vol. 89, p. 187902, Oct. 2002. [Online]. Available: http://link.aps.org/doi/10.1103/PhysRevLett.89.187902

[11] R. A. Malaney, "Location-dependent communications using quantum entanglement," *Phys. Rev. A*, vol. 81, p. 042319, Apr. 2010. [Online]. Available: http://link.aps.org/doi/10.1103/PhysRevA.81.042319

[12] P. A. Dirac, *The Principles of Quantum Mechanics*. London, U.K.: Oxford Univ. Press, 1982.

[13] P. W. Shor, "Scheme for reducing decoherence in quantum computer memory," *Phys. Rev. A*, vol. 52, no. 4, pp. R2493–R2496, Oct. 1995. [Online]. Available: http://dx.doi.org/10.1103/PhysRevA.52.R2493

[14] J. Preskill, "Battling decoherence: The fault-tolerant quantum computer," *Phys. Today*, vol. 52, no. 6, pp. 24–32, 1999.

[15] R. G. Gallager, "Low-density parity-check codes," *IRE Trans. Inf. Theory*, vol. 8, no. 1, pp. 21–28, Jan. 1962.

[16] D. J. C. MacKay, "Good error-correcting codes based on very sparse matrices," *IEEE Trans. Inf. Theory*, vol. 45, no. 2, pp. 399–431, Mar. 1999.

[17] S.-Y. Chung, G. D. Forney, Jr., T. J. Richardson, and R. Urbanke, "On the design of low-density parity-check codes within 0.0045 dB of the Shannon limit," *IEEE Commun. Lett.*, vol. 5, no. 2, pp. 58–60, Feb. 2001.

[18] N. Bonello, S. Chen, and L. Hanzo, "Low-density parity-check codes and their rateless relatives," *IEEE Commun. Surveys Tuts.*, vol. 13, no. 1, pp. 3–26, 2011.

[19] N. Bonello, S. Chen, and L. Hanzo, "Design of low-density parity-check codes," *IEEE Veh. Technol. Mag.*, vol. 6, no. 4, pp. 16–23, Dec. 2011.

[20] D. Gottesman, "Class of quantum error-correcting codes saturating the quantum Hamming bound," *Phys. Rev. A*, vol. 54, no. 3, pp. 1862–1868, Sep. 1996.

[21] D. Gottesman, "Stabilizer codes and quantum error correction," Ph.D. dissertation, California Inst. Technol., Pasadena, CA, USA, 1997.

[22] Z. Babar, P. Botsinis, D. Alanis, S. X. Ng, and L. Hanzo, "The road from classical to quantum codes: A hashing bound approaching design procedure," *IEEE Access*, vol. 3, pp. 146–176, 2015.

[23] H. Wymeersch, F. Penna, and V. Savić, "Uniformly reweighted belief propagation: A factor graph approach," in *Proc. IEEE Int. Symp. Inf. Theory (ISIT)*, Jul./Aug. 2011, pp. 2000–2004.

[24] H. Wymeersch, F. Penna, and V. Savić, "Uniformly reweighted belief propagation for estimation and detection in wireless networks," *IEEE Trans. Wireless Commun.*, vol. 11, no. 4, pp. 1587–1595, Apr. 2012.

[25] M. A. Nielsen and I. L. Chuang, *Quantum Computation and Quantum Information*. Cambridge, U.K.: Cambridge Univ. Press, 2000.

[26] Z. Babar, S. X. Ng, and L. Hanzo, "Reduced-complexity syndrome-based TTCM decoding," *IEEE Commun. Lett.*, vol. 17, no. 6, pp. 1220–1223, Jun. 2013.

[27] E. Pelchat and D. Poulin, "Degenerate Viterbi decoding," *IEEE Trans. Inf. Theory*, vol. 59, no. 6, pp. 3915–3921, Jun. 2013.

[28] R. Cleve, "Quantum stabilizer codes and classical linear codes," *Phys. Rev. A*, vol. 55, pp. 4054–4059, Jun. 1997. [Online]. Available: http://link.aps.org/doi/10.1103/PhysRevA.55.4054

[29] D. MacKay, G. Mitchison, and P. McFadden, "Sparse-graph codes for quantum error correction," *IEEE Trans. Inf. Theory*, vol. 50, no. 10, pp. 2315–2330, Oct. 2004.

[30] A. R. Calderbank and P. W. Shor, "Good quantum error-correcting codes exist," *Phys. Rev. A*, vol. 54, no. 2, pp. 1098–1105, Aug. 1996.

[31] A. Steane, "Multiple-particle interference and quantum error correction," *Proc. R. Soc. Lond. A, Math., Phys. Eng. Sci.*, vol. 452, pp. 2551–2577, Nov. 1996.

[32] A. M. Steane, "Error correcting codes in quantum theory," *Phys. Rev. Lett.*, vol. 77, no. 5, pp. 793–797, Jul. 1996.

[33] A. R. Calderbank, E. M. Rains, P. W. Shor, and N. J. A. Sloane, "Quantum error correction via codes over GF(4)," *IEEE Trans. Inf. Theory*, vol. 44, no. 4, pp. 1369–1387, Jul. 1998.

[34] G. Bowen, "Entanglement required in achieving entanglement-assisted channel capacities," *Phys. Rev. A*, vol. 66, p. 052313, Nov. 2002. [Online]. Available: http://link.aps.org/doi/10.1103/PhysRevA.66.052313

[35] T. A. Brun, I. Devetak, and M.-H. Hsieh, "Correcting quantum errors with entanglement," *Science*, vol. 314, no. 5798, pp. 436–439, Oct. 2006.

[36] T. A. Brun, I. Devetak, and M.-H. Hsieh, "General entanglement-assisted quantum error-correcting codes," in *Proc. IEEE Int. Symp. Inf. Theory*, Jun. 2007, pp. 2101–2105.

[37] M.-H. Hsieh, I. Devetak, and T. Brun, "General entanglement-assisted quantum error-correcting codes," *Phys. Rev. A*, vol. 76, p. 062313, Dec. 2007. [Online]. Available: http://link.aps.org/doi/10.1103/PhysRevA.76.062313

[38] C. H. Bennett and S. J. Wiesner, "Communication via one- and two-particle operators on Einstein-Podolsky-Rosen states," *Phys. Rev. Lett.*, vol. 69, no. 20, pp. 2881–2884, 1992. [Online]. Available: http://dx.doi.org/%7B10.1103/PhysRevLett.69.2881%7D

[39] M. S. Postol. (2001). "A proposed quantum low density parity check code." [Online]. Available: http://arxiv.org/abs/quant-ph/0108131

[40] S. A. Aly, "A class of quantum LDPC codes constructed from finite geometries," in *Proc. IEEE Global Telecommun. Conf.*, Nov./Dec. 2008, pp. 1–5.

[41] Y. Kou, S. Lin, and M. P. C. Fossorier, "Low-density parity-check codes based on finite geometries: A rediscovery and new results," *IEEE Trans. Inf. Theory*, vol. 47, no. 7, pp. 2711–2736, Nov. 2001.

[42] I. B. Djordjevic, "Quantum LDPC codes from balanced incomplete block designs," *IEEE Commun. Lett.*, vol. 12, no. 5, pp. 389–391, May 2008.

[43] B. Vasic and O. Milenkovic, "Combinatorial constructions of low-density parity-check codes for iterative decoding," *IEEE Trans. Inf. Theory*, vol. 50, no. 6, pp. 1156–1176, Jun. 2004.

[44] B. Ammar, B. Honary, Y. Kou, J. Xu, and S. Lin, "Construction of low-density parity-check codes based on balanced incomplete block designs," *IEEE Trans. Inf. Theory*, vol. 50, no. 6, pp. 1257–1269, Jun. 2004.

[45] D. J. C. MacKay, G. Mitchison, and A. Shokrollahi. (2007). *More Sparse-Graph Codes for Quantum Error-Correction*. [Online]. Available: http://www.inference.phy.cam.ac.uk/mackay/cayley.pdf

[46] A. Couvreur, N. Delfosse, and G. Zémor, "A construction of quantum LDPC codes from Cayley graphs," in *Proc. IEEE Int. Symp. Inf. Theory*, Jul./Aug. 2011, pp. 643–647.

[47] A. Couvreur, N. Delfosse, and G. Zemor, "A construction of quantum LDPC codes from Cayley graphs," *IEEE Trans. Inf. Theory*, vol. 59, no. 9, pp. 6087–6098, Sep. 2013.

[48] A. Y. Kitaev, "Fault-tolerant quantum computation by anyons," *Ann. Phys.*, vol. 303, no. 1, pp. 2–30, Jan. 2003. [Online]. Available: http://www.sciencedirect.com/science/article/pii/S0003491602000180

[49] H. Bombin and M. A. Martin-Delgado, "Homological error correction: Classical and quantum codes," *J. Math. Phys.*, vol. 48, no. 5, p. 052105, 2007. [Online]. Available: http://scitation.aip.org/content/aip/journal/jmp/48/5/10.1063/1.2731356

[50] H. Bombin and M. A. Martin-Delgado, "Topological quantum distillation," *Phys. Rev. Lett.*, vol. 97, no. 18, p. 180501, Oct. 2006. [Online]. Available: http://link.aps.org/doi/10.1103/PhysRevLett.97.180501

[51] A. A. Kovalev and L. P. Pryadko, "Quantum Kronecker sum-product low-density parity-check codes with finite rate," *Phys. Rev. A*, vol. 88, p. 012311, Jul. 2013. [Online]. Available: http://link.aps.org/doi/10.1103/PhysRevA.88.012311

[52] J.-P. Tillich and G. Zemor, "Quantum LDPC codes with positive rate and minimum distance proportional to the square root of the blocklength," *IEEE Trans. Inf. Theory*, vol. 60, no. 2, pp. 1193–1202, Feb. 2014.

[53] S. Bravyi and M. B. Hastings, "Homological product codes," in *Proc. 46th Annu. ACM Symp. Theory Comput. (STOC)*, New York, NY, USA, 2014, pp. 273–282. [Online]. Available: http://doi.acm.org/10.1145/2591796.2591870

[54] A. Leverrier, J.-P. Tillich, and G. Zémor. (2015). "Quantum expander codes." [Online]. Available: http://arxiv.org/abs/1504.00822

[55] H. Lou and J. Garcia-Frias, "Quantum error-correction using codes with low-density generator matrix," in *Proc. IEEE 6th Workshop Signal Process. Adv. Wireless Commun.*, Jun. 2005, pp. 1043–1047.

[56] H. Lou and J. Garcia-Frias, "On the application of error-correcting codes with low-density generator matrix over different quantum channels," in *Proc. Int. ITG-Conf. Sour. Channel Coding*, Apr. 2006, pp. 1–6.

[57] S. ten Brink, "Code doping for triggering iterative decoding convergence," in *Proc. IEEE Int. Symp. Inf. Theory*, Jun. 2001, p. 235.

[58] M. Hagiwara and H. Imai, "Quantum quasi-cyclic LDPC codes," in *Proc. IEEE Int. Symp. Inf. Theory*, Jun. 2007, pp. 806–810.

[59] M. Hagiwara and H. Imai. (Aug. 2010). "Quantum quasi-cyclic LDPC codes." [Online]. Available: http://arxiv.org/abs/quant-ph/0701020

[60] M. Hagiwara, K. Kasai, H. Imai, and K. Sakaniwa, "Spatially coupled quasi-cyclic quantum LDPC codes," in *Proc. IEEE Int. Symp. Inf. Theory*, Jul./Aug. 2011, pp. 638–642.

[61] K. Kasai, M. Hagiwara, H. Imai, and K. Sakaniwa, "Non-binary quasi-cyclic quantum LDPC codes," in *Proc. IEEE Int. Symp. Inf. Theory*, Jul./Aug. 2011, pp. 653–657.

[62] K. Kasai, M. Hagiwara, H. Imai, and K. Sakaniwa, "Quantum error correction beyond the bounded distance decoding limit," *IEEE Trans. Inf. Theory*, vol. 58, no. 2, pp. 1223–1230, Feb. 2012.

IEEE Access
The journal for rapid open access publishing

[63] I. Andriyanova, D. Maurice, and J.-P. Tillich, "Spatially coupled quantum LDPC codes," in *Proc. IEEE Inf. Theory Workshop*, Sep. 2012, pp. 327–331.

[64] D. Maurice, J.-P. Tillich, and I. Andriyanova, "A family of quantum codes with performances close to the hashing bound under iterative decoding," in *Proc. IEEE Int. Symp. Inf. Theory*, Jul. 2013, pp. 907–911.

[65] T. Camara, H. Ollivier, and J.-P. Tillich. (2005). "Constructions and performance of classes of quantum LDPC codes." [Online]. Available: http://arxiv.org/abs/quant-ph/0502086

[66] T. Camara, H. Ollivier, and J.-P. Tillich, "A class of quantum LDPC codes: Construction and performances under iterative decoding," in *Proc. IEEE Int. Symp. Inf. Theory*, Jun. 2007, pp. 811–815.

[67] M.-H. Hsieh, T. A. Brun, and I. Devetak, "Entanglement-assisted quantum quasicyclic low-density parity-check codes," *Phys. Rev. A*, vol. 79, p. 032340, Mar. 2009. [Online]. Available: http://link.aps.org/doi/10.1103/PhysRevA.79.032340

[68] M.-H. Hsieh, W.-T. Yen, and L.-Y. Hsu. (2009). "Performance of entanglement-assisted quantum LDPC codes constructed from finite geometries." [Online]. Available: http://arxiv-web3.library.cornell.edu/abs/0906.5532v1

[69] M.-H. Hsieh, W.-T. Yen, and L.-Y. Hsu, "High performance entanglement-assisted quantum LDPC codes need little entanglement," *IEEE Trans. Inf. Theory*, vol. 57, no. 3, pp. 1761–1769, Mar. 2011.

[70] P. Tan and J. Li, "Efficient quantum stabilizer codes: LDPC and LDPC-convolutional constructions," *IEEE Trans. Inf. Theory*, vol. 56, no. 1, pp. 476–491, Jan. 2010.

[71] I. B. Djordjevic, "Photonic entanglement-assisted quantum low-density parity-check encoders and decoders," *Opt. Lett.*, vol. 35, no. 9, pp. 1464–1466, May 2010. [Online]. Available: http://ol.osa.org/abstract.cfm?URI=ol-35-9-1464

[72] Y. Fujiwara, D. Clark, P. Vandendriessche, M. De Boeck, and V. D. Tonchev, "Entanglement-assisted quantum low-density parity-check codes," *Phys. Rev. A*, vol. 82, p. 042338, Oct. 2010. [Online]. Available: http://link.aps.org/doi/10.1103/PhysRevA.82.042338

[73] Y. Fujiwara and V. D. Tonchev, "A characterization of entanglement-assisted quantum low-density parity-check codes," *IEEE Trans. Inf. Theory*, vol. 59, no. 6, pp. 3347–3353, Jun. 2013.

[74] Y. Fujiwara, A. Gruner, and P. Vandendriessche, "High-rate quantum low-density parity-check codes assisted by reliable qubits," *IEEE Trans. Inf. Theory*, vol. 61, no. 4, pp. 1860–1878, Apr. 2015.

[75] R. Laflamme, C. Miquel, J. P. Paz, and W. H. Zurek, "Perfect quantum error correcting code," *Phys. Rev. Lett.*, vol. 77, pp. 198–201, Jul. 1996. [Online]. Available: http://link.aps.org/doi/10.1103/PhysRevLett.77.198

[76] T. J. Richardson, M. A. Shokrollahi, and R. L. Urbanke, "Design of capacity-approaching irregular low-density parity-check codes," *IEEE Trans. Inf. Theory*, vol. 47, no. 2, pp. 619–637, Feb. 2001.

[77] Y. Fujiwara, "Quantum error correction via less noisy qubits," *Phys. Rev. Lett.*, vol. 110, p. 170501, Apr. 2013. [Online]. Available: http://link.aps.org/doi/10.1103/PhysRevLett.110.170501

[78] D. J. C. MacKay, *Information Theory, Inference and Learning Algorithms*. Cambridge, U.K.: Cambridge Univ. Press, 2003.

[79] E. Berlekamp, R. J. McEliece, and H. C. A. Van Tilborg, "On the inherent intractability of certain coding problems (Corresp.)," *IEEE Trans. Inf. Theory*, vol. 24, no. 3, pp. 384–386, May 1978.

[80] T. J. Richardson and R. L. Urbanke, "The capacity of low-density parity-check codes under message-passing decoding," *IEEE Trans. Inf. Theory*, vol. 47, no. 2, pp. 599–618, Feb. 2001.

[81] D. Poulin and Y. Chung, "On the iterative decoding of sparse quantum codes," *Quantum Inf. Comput.*, vol. 8, no. 10, pp. 987–1000, Nov. 2008. [Online]. Available: http://dl.acm.org/citation.cfm?id=2016985.2016993

[82] D. A. Lidar and T. A. Brun, *Quantum Error Correction*. Cambridge, U.K.: Cambridge Univ. Press, 2013. [Online]. Available: http://books.google.co.uk/books?id=XV9sAAAAQBAJ

[83] Y.-J. Wang, B. C. Sanders, B.-M. Bai, and X.-M. Wang, "Enhanced feedback iterative decoding of sparse quantum codes," *IEEE Trans. Inf. Theory*, vol. 58, no. 2, pp. 1231–1241, Feb. 2012.

[84] M. J. Wainwright, T. S. Jaakkola, and A. S. Willsky, "A new class of upper bounds on the log partition function," *IEEE Trans. Inf. Theory*, vol. 51, no. 7, pp. 2313–2335, Jul. 2005.

[85] T. G. Roosta, M. J. Wainwright, and S. S. Sastry, "Convergence analysis of reweighted sum-product algorithms," *IEEE Trans. Signal Process.*, vol. 56, no. 9, pp. 4293–4305, Sep. 2008.

[86] J. Liu and R. C. de Lamare, "Knowledge-aided reweighted belief propagation decoding for regular and irregular LDPC codes with short blocks," in *Proc. Int. Symp. Wireless Commun. Syst. (ISWCS)*, Aug. 2012, pp. 984–988.

[87] J. Liu and R. C. de Lamare, "Low-latency reweighted belief propagation decoding for LDPC codes," *IEEE Commun. Lett.*, vol. 16, no. 10, pp. 1660–1663, Oct. 2012.

[88] J. Liu, R. C. de Lamare, and H. Wymeersch, "Locally-optimized reweighted belief propagation for decoding finite-length LDPC codes," in *Proc. IEEE Wireless Commun. Netw. Conf. (WCNC)*, Apr. 2013, pp. 4311–4316.

[89] H. Wymeersch, F. Penna, V. Savić, and J. Zhao, "Comparison of reweighted message passing algorithms for LDPC decoding," in *Proc. IEEE Int. Conf. Commun. (ICC)*, Jun. 2013, pp. 3264–3269.

ZUNAIRA BABAR received the B.Eng. degree in electrical engineering from the National University of Science and Technology, Islamabad, Pakistan, in 2008, and the M.Sc. (Hons.) and Ph.D. degrees in wireless communications from the University of Southampton, U.K., in 2011 and 2015, respectively.

Her research interests include quantum error correction codes, channel coding, coded modulation, iterative detection, and cooperative communications.

PANAGIOTIS BOTSINIS (S'12) received the M.Eng. degree from the School of Electrical and Computer Engineering, National Technical University of Athens, Greece, in 2010, and the M.Sc. (Hons.) and Ph.D. degrees in wireless communications from the University of Southampton, U.K., in 2011 and 2015, respectively. Since 2010, he has been a member of the Technical Chamber of Greece. He is currently a Research Fellow with the Southampton Wireless Group, School of Electronics and Computer Science, University of Southampton.

His research interests include quantum-assisted communications, quantum computation, iterative detection, OFDM, MIMO, multiple access systems, coded modulation, channel coding, cooperative communications, and combinatorial optimization. AQ:9

DIMITRIOS ALANIS (S'13) received the M.Eng. degree in electrical and computer engineering from the Aristotle University of Thessaloniki, in 2011, and the M.Sc. degree in wireless communications from the University of Southampton, in 2012, where he is currently pursuing the Ph.D. degree with the Southampton Wireless Group, School of Electronics and Computer Science.

His research interests include quantum computation and quantum information theory, quantum search algorithms, cooperative communications, resource allocation for self-organizing networks, bioinspired optimization algorithms, and classical and quantum game theory.

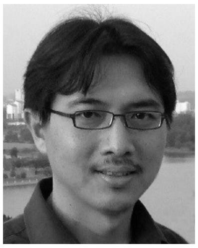

SOON XIN NG (S'99–M'03–SM'08) received the B.Eng. (Hons.) degree in electronics engineering and the Ph.D. degree in wireless communications from the University of Southampton, Southampton, U.K., in 1999 and 2002, respectively. From 2003 to 2006, he was a Post-Doctoral Research Fellow working on collaborative European research projects known as SCOUT, NEWCOM, and PHOENIX. Since 2006, he has been a member of the Academic Staff with the School of Electronics and Computer Science, University of Southampton. He is currently involved in the OPTIMIX and CONCERTO European projects and the IUATC and UC4G projects. He is an Associate Professor of Telecommunications with the University of Southampton. He has authored over 180 papers and co-authored two John Wiley/IEEE Press books in his research field.

His research interests include adaptive coded modulation, coded modulation, channel coding, space-time coding, joint source and channel coding, iterative detection, OFDM, MIMO, cooperative communications, distributed coding, quantum error correction codes, and joint wireless-and-optical-fiber communications. He is a Chartered Engineer and fellow of the Higher Education Academy, U.K.

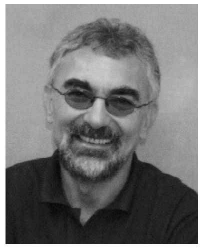

LAJOS HANZO (M'91–SM'92–F'04) received the degree in electronics in 1976, the Ph.D. degree in 1983, and the Doctor Honoris Causa degree from the Technical University of Budapest, in 2009. During his 38-year career in telecommunications, he has held various research and academic positions in Hungary, Germany, and the U.K. Since 1986, he has been with the School of Electronics and Computer Science, University of Southampton, U.K., as the Chair in Telecommunications. He has successfully supervised 100 Ph.D. students, co-authored 20 John Wiley/IEEE Press books in mobile radio communications totaling in excess of 10 000 pages, authored over 1500 research entries at the IEEE Xplore, acted as the TPC Chair and General Chair of the IEEE conferences, presented keynote lectures, and received a number of distinctions. He is directing 100 strong academic research teams, working on a range of research projects in the field of wireless multimedia communications sponsored by the industry, the Engineering and Physical Sciences Research Council, U.K., the European Research Council's Advanced Fellow Grant, and the Royal Society's Wolfson Research Merit Award. He is an enthusiastic supporter of industrial and academic liaison and offers a range of industrial courses.

He is a fellow of the Royal Academy of Engineering, the Institution of Engineering and Technology, and the European Association for Signal Processing. He is also a Governor of the IEEE VTS. From 2008 to 2012, he was the Editor-in-Chief of the *IEEE Press* and a Chaired Professor with Tsinghua University, Beijing. He has over 22 000 citations.

• • •

AUTHOR QUERIES

AQ:1 = Please check whether the edits made in the financial section are OK.
AQ:2 = Table 1 and its citation are missed in the provided manuscript. So other tables and their corresponding citations have been renumbered in the proof. Please check and confirm that they are fine as set.
AQ:3 = Please provide the issue no. for ref. [1].
AQ:4 = Please provide the issue no. and month for refs. [2]–[4] and [22].
AQ:5 = Please provide the month. Also confirm the issue no. for ref. [5].
AQ:6 = Please provide the month for ref. [18].
AQ:7 = Please provide the department name for ref. [21].
AQ:8 = Please confirm the author name ‘‘V. Savić’’ is correct in throughout references.
AQ:9 = Please provide the expansion for the acronyms ‘‘OFDM and MIMO.’’